Flooding Frequency and Afterstorm Dune Recovery in Cedar Lakes' Washover

by

Abolfazl Yousefi, Orencio Duran Vinent

abolfazl_yousefi@tamu.edu oduranvinent@tamu.edu

Final Project Report Contract no. 24-022-002-E011





This report was funded in part by a Texas Coastal Management Program grant approved by the Texas Land Commissioner, providing financial assistance under the Coastal Zone Management Act of 1972, as amended, awarded by the National Oceanic and Atmospheric Administration (NOAA), Office for Coastal Management, pursuant to NOAA Award No. NA23NOS4190249. The views expressed herein are those of the author(s) and do not necessarily reflect the views of NOAA, the U.S. Department of Commerce, or any of their subagencies.

Contents

Ta	able (of Contents	i			
1	Introduction					
2	Con	ompile Existing Data				
	2.1	Hydrodynamic and Meteorological Data: Tides, Waves, Weather	5			
	2.2	Morphological Data: DEMs	7			
3	Met	thods and Modeling Approach	8			
	3.1	Calculation of Barrier and Dune Morphological Characteristics	8			
	3.2	Calculation of Reference Beach Elevation	10			
	3.3	Calculation of Total Water Level (TWL) at the Beach	10			
	3.4	Calculation of Maximum Sand Transport Rate at the Beach	11			
	3.5	After-Storm Dune Recovery	14			
4	Site	e Description	15			
	4.1	Topographic data and Growth Rate Analysis	15			
	4.2	Morphological Characteristics	22			
		4.2.1 Barrier Characteristics	22			
		4.2.2 Dune Morphological Evolution	24			
		4.2.3 Evolution of the Length of the Dry Beach and Relation to Dune Size	27			
	4.3	Sediment Budget and Elevation Change Rates	30			
		4.3.1 Elevation Change Rates	30			
		4.3.2 Beach and Dune Sediment Budget	33			

5	Mo	del Prediction	36				
	5.1	High-Water Event (HWE) flooding	36				
	5.2	Statistical Properties of HWE	40				
	5.3	Sediment Transport	42				
	5.4	After-Storm Dune Recovery	43				
		5.4.1 Barrier elevation capital	43				
		5.4.2 Validation of the Dune Recovery Threshold	46				
	5.5	Barrier Breaching Threshold	47				
	5.6	Quantification of Dune Recovery and Barrier Breaching for Different Sea Level Rise Scenarios	49				
		5.6.1 First Approach	50				
		5.6.2 Second Approach	51				
Li	ist of Figures 56						
$_{ m Li}$	ist of Tables 63						

Summary

The narrow coastal barrier in front of Cedar Lakes, Texas, near Sargent Beach, is prone to frequent overwash and occasional breaching, most recently during Hurricane Harvey. We assessed the stability of the coastal dunes and the broader barrier system by analyzing natural dune formation, erosion, and recovery. Below, we summarize our findings regarding barrier morphology and growth rates, flooding frequency, dune recovery and elevation capital, breaching susceptibility, and future vulnerabilities under different sea level rise (SLR) scenarios. All elevation and water level values presented in this summary are referenced to Mean Sea Level (MSL).

Barrier, dune, and beach morphology and growth rates: We identified three distinct morphological regions across the site: (1) the west side, characterized by a poorly developed dune system; (2) the washover region, which lacked dunes due to consistent overwash activity; and (3) the east side, exhibiting well-developed dunes and providing greater stability.

Average primary dune heights across the site ranged from 1.8 m to 2.0 m (relative to MSL). In 2009, the modal dune heights were approximately 1.6 m on the west side and 1.9 m on the east side, reflecting the most frequently occurring values in each region. By 2012, these modal heights increased to 1.7 m and 2.3 m, respectively. Over the same period, the barrier width expanded from 90 m in 2009 to 120 m in 2019, primarily due to shoreline accretion following Hurricane Harvey. The primary dune width remained relatively stable, consistently ranging between 20 and 30 m. Initially, a single primary dune system existed across the site; however, as shoreline accretion progressed after Hurricane Harvey, a secondary dune system began to form, most prominently on the east side.

The average dune growth rate over the entire period was approximately $0.2\,\mathrm{m/yr}$, although newly formed dunes experienced growth rates up to $0.9\,\mathrm{m/yr}$ after Hurricane Harvey. Aeolian transport was the main driver of dune growth, and we found the maximum potential sediment transport rate to be $12.5\,\mathrm{m^2/yr}$, calculated from available wind data. Following Hurricane Harvey, the beach recovered at a maximum rate of $0.5\,\mathrm{m/yr}$.

Flooding patterns and exposure: The daily maximum total water level exceeded 1 m every month. The dune base elevation (1.5 m) was overtopped every four months. Elevations of 2 m were exceeded annually, while the maximum dune height (2.7 m) was exceeded once every ten years. In terms of spatial exposure, the washover region was submerged 10% of the time, while dunes with elevations above the average dune height (1.9 m) were submerged only about 0.1% of the time.

Dune recovery and elevation capital: In this study, we used elevation capital as a key indicator of dune recovery, defined as the elevation of the barrier excluding dunes. A model was used to predict a threshold for elevation capital below which dunes, on average, cannot recover. This threshold was determined based on the maximum growth rate of new dunes and the frequency of flooding. The model predicted a threshold of 1.25 m (relative to MSL), which was consistent with the value derived from available data during Hurricane

Harvey $(1.25 \,\mathrm{m})$. Therefore, the overwash region remains active, as elevations in this area persist below the recovery threshold, inhibiting dune formation and sustaining frequent overwash events. The dune recovery threshold elevation $(1.25 \,\mathrm{m})$ was flooded approximately every two months.

Tentative condition for barrier breaching: We found that barriers with widths below 70 m were susceptible to breaching during Hurricane Harvey, even when elevation capital exceeded the dune recovery threshold.

Model predictions for future dune recovery: We quantified dune recovery and barrier breaching using two key metrics: the fraction of the barrier where dunes can recover and the fraction susceptible to breaching after an overwash.

We analyzed SLR scenarios based on projections for 2050, with rates of 1.0 cm/yr, 1.5 cm/yr, and 2.0 cm/yr representing moderate, high, and extreme scenarios, respectively, relative to the year 2000, based on NOAA estimates. The current local SLR rate for the region is approximately 6.6 mm/yr.

We applied these SLR scenarios to evaluate dune recovery and barrier breaching under future conditions using two distinct approaches:

- In the first approach, the entire barrier undergoes passive inundation while maintaining a constant width. This results in a gradual reduction of elevation capital over time, limiting dune recovery.
 - By 2050, the fraction of the barrier where dunes can recover is projected to be 35%, 18%, and 0% under the moderate, high, and extreme SLR scenarios, respectively.
- In the second approach, the beach and primary dune adjust to SLR, while the back-barrier experiences passive inundation, leading to changes in barrier width. Unlike the first approach, where width remains constant, the evolving morphology influences the barrier's susceptibility to breaching.
 - By 2050, the dune recovery fraction remains slightly higher than in the first approach, at 46%, 19%, and 16%, respectively. However, the fraction of the barrier at risk of breaching increases, reaching 33%, 78%, and 87% under the respective SLR scenarios.

Ideal conditions for dune growth in the Project area: Our model and data analysis suggests two main conditions for dune growth. The first is the after-storm dune recovery condition, given by a local elevation capital (averaged over at least 50m of alongshore length) ideally above 1.3m relative to MSL. This means that at least 50 meters of the cross-shore barrier has to have elevations higher than 1.3m.

The second is a condition to have relatively larger-than-average mature dunes (around 2.5m above MSL) and is given by the distance from the location at the beach with an elevation equal to the characteristic beach elevation ($Z_r = 1$ m) and the dune crest: this beach-to-dune crest distance should be above 40m for relatively tall dunes to develop. Since this distance characterizes the length of the dry-sand beach, this condition is related to the availability of dry sand needed for an effective wind-driven transport and dune formation.

1 Introduction

The narrow coastal barrier in front of Cedar Lakes, Texas (Fig. 1), near Sargent Beach, is prone to frequent overwash and occasional breaching, most recently during Hurricane Harvey (Fig. 2). This project explores the resilience of this site, and in particular its coastal dunes, by investigating natural dune formation, erosion, and recovery at and around the washover fan.



Figure 1: Location of the study area (A). Satellite view of the study area (B).

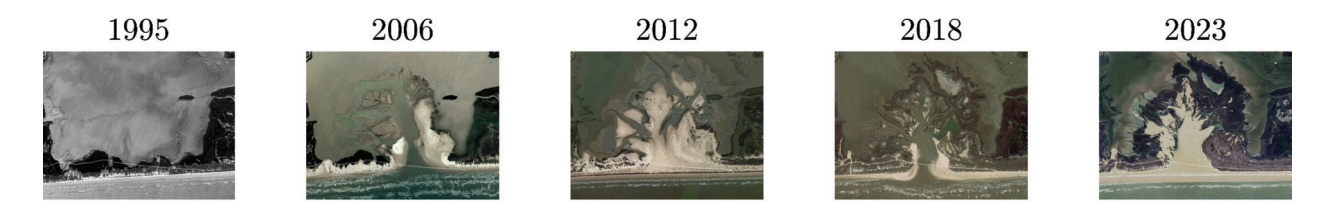


Figure 2: Time evolution of the Cedar Lakes washover site illustrating dynamic inlet formation and closure over nearly three decades (1995–2023). The sequence of aerial images highlights periods of inlet breaching, sediment deposition, and subsequent natural recovery, emphasizing the transient nature of barrier island morphology. These changes are driven by storm-induced overwash, wave run-up, and sediment transport processes. Understanding these morphological shifts is critical for validating dune recovery models, estimating wave run-up intensity, and assessing coastal resiliency. This site serves as a foundational case study for evaluating the interplay between flooding frequency, after-storm dune recovery, and long-term barrier island stability along the Texas coast.

In this document, we summarize the deliverables of Task 4 and present selected results from our analysis.

Section 2 describes all the data compiled for this study, including digital elevation models (DEMs), wind velocity, precipitation, storm impacts, offshore wave data, water gauge data, and satellite and shoreline change data (Figure 3 and Table 1).

Section 3 outlines the method and modeling approach used for data analysis and the estimation of derived quantities. This includes the calculation of barrier and dune morphological characteristics (Section 3.1), reference beach elevation (Section 3.2), total water level (TWL) at the beach (Section 3.3), maximum sand transport rate at the beach (Section 3.4), and a description of the stochastic model (Section 3.5).

Section 4 presents a detailed site description of the Cedar Lakes based on historical topographic data and DEM analyses. It includes topographic maps and growth rate analyses (Section 4.1), as well as quantitative assessments of morphological features such as barrier (Section 4.2.1), and dunes (Section 4.2.2). The section also covers sediment dynamics and elevation change rates (Section 4.3), highlighting spatial and temporal trends in coastal morphology and sediment budgets.

Section 5 introduces model predictions and key thresholds relevant to storm-driven coastal change. It includes an analysis of high-water event (HWE) flooding (Section 5.1), sediment transport patterns (Section 5.3), and after-storm dune recovery dynamics (Section 5.4). The section also defines and validates thresholds for dune recovery (Section 5.4.2) and barrier breaching (Section 5.5). Lastly, it presents projections of dune recovery and barrier breaching under different SLR scenarios through 2050 (Section 5.6).

2 Compile Existing Data

The initial phase of the project focused on aggregating relevant data from publicly available sources. The data included satellite imagery to track temporal landscape changes, DEMs, and LiDAR data—key resources for accurate geomorphological assessments. In addition, water level records and offshore wave data were gathered to analyze hydrodynamic conditions, while weather data was collected to provide insights into atmospheric variables affecting the coastal area.

Figure 3 shows the timelines for the various datasets collected, highlighting their periods of availability. The focus was primarily on data from stations near Cedar Lakes. The red dashed lines in the timeline indicate the availability of DEMs and LiDAR data. Sections 2.1 and 2.2 provide more detailed explanations of the collected information.

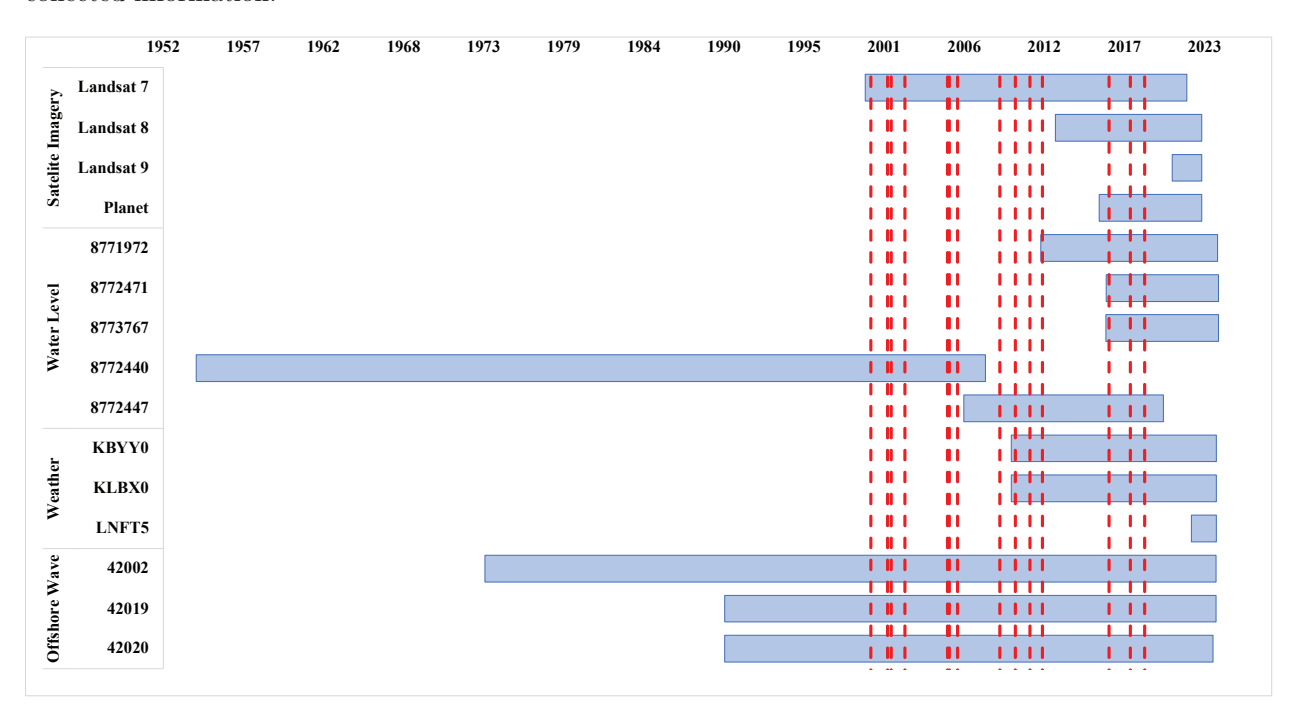


Figure 3: Timeline of available data from various sources for stations near Cedar Lakes, TX, including satellite imagery, water level records, weather observations, and offshore wave data. Red dashed lines indicate the periods when DEMs and LiDAR data were collected.

2.1 Hydrodynamic and Meteorological Data: Tides, Waves, Weather

Tidal, wave, and weather datasets were generally available at hourly intervals. However, some stations initially recorded at higher frequencies—up to four samples per hour. For consistency, all tidal, wave, and weather data were synchronized to an hourly temporal resolution by selecting the first value of each hour from the higher-frequency recordings. Tidal data were normalized to MSL, accounting for long-term sea

level trends to avoid bias in the analysis.

Figure 4 illustrates the locations of the deep-water wave buoys, tidal gauge stations, and weather stations near Cedar Lakes. The specific details of each station, including elevation and duration of data availability, are presented in Table 1.

Table 1: List of station IDs, names, and characteristics for wave buoys, tidal gauges, and weather stations.

Station Type Station ID		Station Name	Elevation (ft)	Time Series Start	Time Series End	Temporal Resolution
	8773767	Matagorda Bay Entrance Channel, TX	14.3	18-Jun-2016	29-Feb-2024	Hourly
	8772471	Freeport Harbor, TX	11.4	28-Jun-2016	29-Feb-2024	Hourly
Tidal Gauge	8772447	Freeport Harbor, TX	26.3	28-Sep-2006	22-May-2020	Hourly
	8772440	Freeport Harbor, TX	N/A	14-Apr-1954	19-Mar-2008	Hourly
	8771972	San Luis Pass, TX	18.5	01-Jan-2012	31-Jan-2024	Hourly
	KBYY0	Bay City / Caney	N/A	01-Jan-2010	01-Jan-2024	Hourly
Weather Station	KLBX0	Angleton / Snipe	N/A	01-Jan-2010	01-Jan-2024	Hourly
	LNFT5	Brazos 451 Oil Platform	N/A	23-Apr-2022	01-Jan-2024	Hourly
	42002	WEST GULF - 207 NM East of Brownsville, TX	13.5	01-Jan-1974	31-Dec-2023	Hourly
Wave Buoy	42019	FREEPORT, TX - 60 NM South of Freeport, TX	10.5	25-May-1990	31-Dec-2023	Hourly
	42020	CORPUS CHRISTI, TX - 60 NM SSE of Corpus Christi, TX	13.5	24-May-1990	11-Oct-2023	Hourly

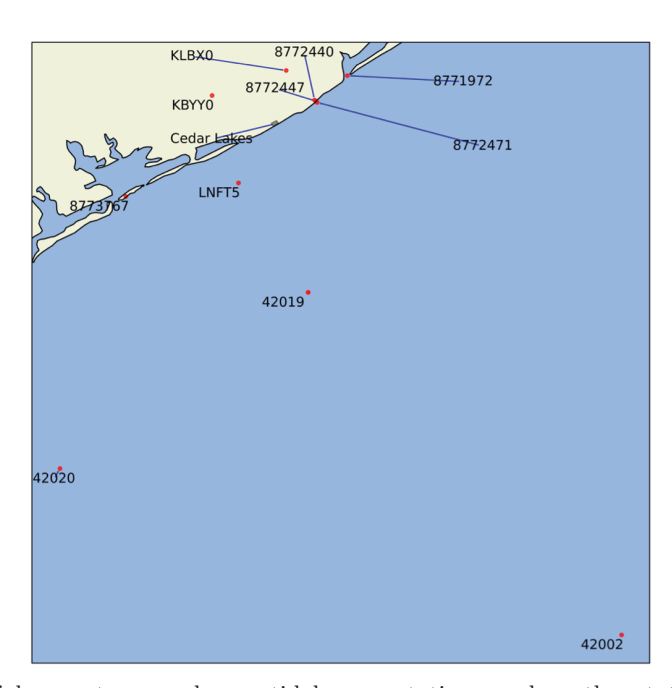


Figure 4: Locations of deep-water wave buoys, tidal gauge stations, and weather stations near Cedar Lakes.

2.2 Morphological Data: DEMs

The DEMs used in this project were obtained from two primary sources:

- NOAA's Office for Coastal Management: High-resolution coastal DEM archives were obtained from NOAA's LiDAR data viewer. The available datasets cover the periods of October 2001, September 2002, March 2009, February 2018, and February 2019.
- 2. **Texas General Land Office (TGLO)**: The TGLO provided additional high-resolution DEM datasets for April 2010, April 2011, and February 2012.

3 Methods and Modeling Approach

3.1 Calculation of Barrier and Dune Morphological Characteristics

Accurate mapping and analysis of coastal barriers and dunes is essential for effective coastal management and erosion mitigation. We used cross-shore elevation profiles derived from available DEMs (Section 2.2) to quantify barrier morphology in terms of height and width, and dune morphology in terms of height, width, and aspect ratio.

To delineate the barrier region, we first needed a threshold elevation that distinguishes water-influenced zones from the rest of the barrier island. For this purpose, we used the beach reference elevation (Z_r) , defined as the characteristic elevation typically flooded by high-water events occurring 18 times per year $(\lambda_r \approx 18 \text{ yr}^{-1}; \text{ see Section 3.2})$. For this site, Z_r was determined to be 1 m. Elevations below 1 m are dominated by water-driven erosion and accretion processes, behaving similarly to shoals. In contrast, areas above this threshold typically remain dry under normal conditions, allowing vegetation growth and thus making 1 m a suitable elevation for delineating barrier island morphology. Therefore, $Z_r = 1$ m was used as the threshold elevation for identifying the barrier region.

A zero-crossing method was applied along each cross-shore profile to identify the points where the elevation intersects the beach reference elevation (Z_r) , defining the lateral limits of the barrier. The barrier width was then calculated as the horizontal distance between these points, while the maximum elevation within this section, relative to Z_r , was recorded as the barrier height.

The primary dune was defined as the first significant crest closest to the sea that exceeds the dune base elevation (0.5 m). This feature was identified using a zero-crossing approach. The dune height was measured as the vertical distance from the crest to its base, relative to Z_r . The dune width was calculated as the horizontal distance between the two zero-crossing points on either side of the crest, where the elevation drops below the 0.5 m dune base threshold.

Figure 5 illustrates these concepts using a cross-shore profile from Cedar Lakes, Texas.

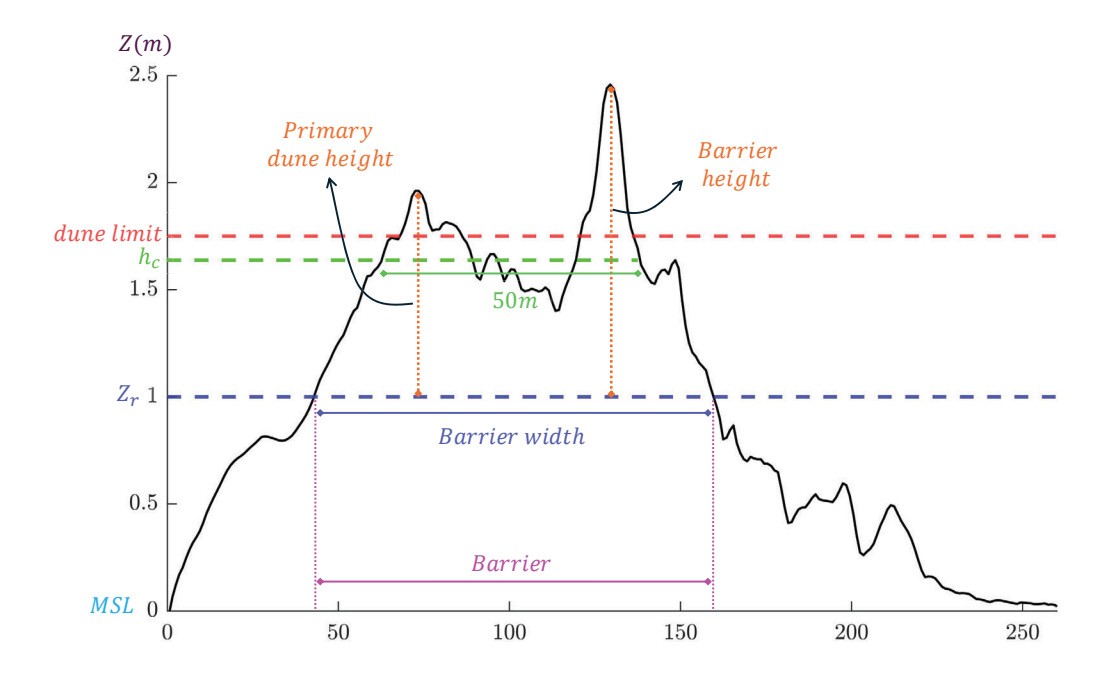


Figure 5: Cross-shore profile in Cedar Lakes, Texas, illustrating key coastal morphology metrics. All elevations are referenced to MSL. The barrier width is measured as the distance between the points where the elevation crosses the 1-meter beach reference elevation (Z_r) , while the barrier height corresponds to the maximum elevation within this section, measured relative to Z_r . The pink vertical dotted lines indicate the lateral limits of the barrier. The primary dune is identified as the first crest exceeding the dune base elevation of 0.5 m, closest to the sea. The elevation capital (h_c) represents the island's characteristic elevation following overwash. The solid green horizontal line illustrates the typical overwash length (50 m).

To provide statistical insights into the morphological features described earlier, we compiled a comprehensive dataset by merging all available data, excluding those from October 2001, September 2002, March 2009, and February 2018. These datasets were omitted due to significant erosion during those periods, which altered both dune and barrier morphology, making them unrepresentative of typical coastal characteristics. Their inclusion would have introduced bias, particularly affecting statistical measures such as the mean and percentile calculations. To further enhance the reliability of the analysis, outliers were identified and removed using the interquartile range (IQR) method.

From this refined dataset, several key statistical measures were computed to characterize the distribution of morphological parameters. The mode, representing the most frequently occurring calculated value, provides insight into the most common characteristics within the dataset. The mean represents the central tendency, reflecting the typical calculated value for each parameter. To assess the distribution of higher values, we determined the 90th percentile (P_{90}) and 75th percentile (P_{75}) , which correspond to the values below which 90% and 75% of the data fall, respectively. Additionally, the maximum value (P_{max}) was identified as the highest computed value within the dataset.

3.2 Calculation of Reference Beach Elevation

The reference beach elevation (Z_r) is defined as the characteristic elevation corresponding to an annualized frequency of high-water events (HWEs) of 18 occurrences per year $(\lambda_r \approx 18 \text{ yr}^{-1})$. This elevation serves as a key indicator of the beach's typical response to recurring HWEs, providing valuable insight into coastal dynamics [5].

To assess how different approaches to handling data gaps influence the estimation of Z_r , we conducted two sets of analyses.

In the first approach, we restricted the dataset to time series with no more than 100 consecutive hours of missing data. This limitation was imposed to preserve data integrity and minimize distortions caused by extended gaps. Missing values were filled using linear interpolation, which could slightly alter the timing of HWEs but did not affect their magnitudes.

In the second approach, we utilized the entire dataset, regardless of gap size, applying linear interpolation to fill all missing values. This method ensured that no valuable information, particularly storm-related events, was omitted and allowed us to explore potential insights that might be lost when using a more restrictive dataset.

For the purpose of estimating Z_r , we used TWL time series generated using the tidal record from Freeport Harbor in combination with wave data from each available buoy (see Section 3.3 and Table 1). This approach allowed us to assess the sensitivity of Z_r estimates to different wave inputs while holding the water level record constant for the site.

3.3 Calculation of Total Water Level (TWL) at the Beach

In this section, we follow the approach of [5].

The TWL at the shoreline (η) is calculated by summing the still water level (η_S) and the 2% exceedance wave runup (η_W) . This equation considers the cumulative impact of tidal fluctuations, wave dynamics, and meteorological phenomena (e.g., storm surges) on shoreline processes, including erosion and flooding.

$$\eta = \eta_S + \eta_W \tag{1}$$

The still water level (η_S) represents the instantaneous average water elevation obtained from tide gauge measurements. It accounts for the contributions of the astronomical tide (A_t) , MSL, and non-tidal residuals, primarily from storm surges. The 2% exceedance wave runup (η_W) describes the elevation caused by wave action, which combines the time-averaged wave setup with the maximum extent of swash motion. This level is only exceeded 2% of the time [6].

To estimate the wave runup, we utilized the equation proposed by [6, 7], which has the form,

$$\eta_W = a(\beta)\sqrt{H_S L_0} \tag{2}$$

which depends on the significant wave height in deep water (H_S) and the deep-water wavelength (L_0) , computed using the deep-water dispersion relation:

$$L_0 = \frac{gT_P^2}{2\pi} \tag{3}$$

where g is the gravity acceleration and T_P is the wave peak period. The factor $a(\beta)$ is function of the beach's foreshore slope β ,

$$a(\beta) = 0.033 \left(\sqrt{1 + 1.2\beta_*^2} + \beta_* \right) \tag{4}$$

Here, $\beta_* = \beta/0.087$ represents a rescaled beach slope. For the purpose of this project, the beach slope β was set to 0.02.

Water level measurements were compiled from three Freeport Harbor tidal gauges (stations 8772471, 8772447, and 8772440; see Table 1) to produce a continuous and extended record of still water levels. These records were merged to create the longest available time series of hourly water level data. Wave data were obtained separately from multiple offshore wave buoys near the study area (see Table 1). These datasets were then used together to calculate time series of TWL $(\eta(t))$. From the resulting TWL time series, daily (η_d) , monthly (η_m) , and yearly (η_y) maximum water levels were identified by selecting the highest value within each respective interval.

3.4 Calculation of Maximum Sand Transport Rate at the Beach

In this section, we follow the approach of [2].

The mobilization of sand particles from a bed occurs when friction velocity u_* exceeds a critical threshold u_t [2].

We calculate the instantaneous transport rate as a function of the squared difference between the friction velocity $(u_*(t)^2)$ and the threshold friction velocity $(u_t(t)^2)$:

$$|\overrightarrow{q_s}(t)| = C\left(u_*(t)^2 - u_t(t)^2\right) \tag{5}$$

Where the coefficient C is a dimensionless proportionality factor that quantifies the effect of particle and fluid density, grain size, and gravitational acceleration on the sediment transport rate, and it can be estimated by:

$$C = 25 \left(\frac{\rho_f}{\rho_p}\right) \sqrt{\frac{d}{g}} \tag{6}$$

Where ρ_p is the density of the sediment particles, ρ_f is the density of the fluid (e.g., air for aeolian transport), d represents the diameter of the sediment particles, and g is the acceleration due to gravity.

The threshold friction velocity is calculated using:

$$u_t \approx 0.1 \sqrt{\frac{\rho_p}{\rho_f} g d} \tag{7}$$

Where d is the grain size, g is the acceleration due to gravity, and ρ_p/ρ_f is the density ratio between the particles and the fluid. Upon inserting the specified values into the equation, where $d=120\,\mu\text{m}$, $\rho_f=1.2\,\text{kg/m}^3$, and $\rho_p=2500\,\text{kg/m}^3$, the resultant threshold friction velocity is approximately $0.15\,\text{m/s}$.

After rearranging the terms to relate the threshold friction velocity to the friction velocity, the equation 5 can be expressed as:

$$|\overrightarrow{q_s}(t)| = Cu_t^2 \left[\left(\frac{u_*(t)}{u_t} \right)^2 - 1 \right]$$
 (8)

Using the derived coefficient C along with the square of the threshold friction velocity u_t^2 , the transport capacity constant Q is calculated from the given parameters:

$$Q = Cu_t^2 = 25 \left(\frac{\rho_p}{\rho_f}\right) \sqrt{\frac{d}{g}} \times 10^{-2} \left(\frac{\rho_p}{\rho_f}\right) gd = 0.25 d\sqrt{gd} = 10^{-6} \text{ m}^2/\text{s} = 32 \text{ m}^2/\text{yr}$$
 (9)

Therefore, the equation 8 can be written as:

$$|\overrightarrow{q_s}(t)| = Q \left[\left(\frac{u_*(t)}{u_t} \right)^2 - 1 \right] \tag{10}$$

With $Q = 32 m^2/yr$.

Assuming $u_*(t)/u_t \approx U(t)/U_t$, where U(t) is the wind velocity obtained from wind data, and U_t is the

threshold wind velocity, the sediment transport rate can be estimated as:

$$|\overrightarrow{q_s}(t)| = Q\left[\left(\frac{U_{(t)}}{U_t}\right)^2 - 1\right]\Theta\left(U_{(t)} > U_t\right)$$
(11)

The function $\Theta(U(t) > U_t)$ is the Heaviside step function, which is equal to 0 when $U(t) < U_t$ and 1 when $U(t) > U_t$. The use of the Heaviside function ensures that the sediment transport rate is only calculated when the wind velocity is sufficient to move sediment (see Figure 6).

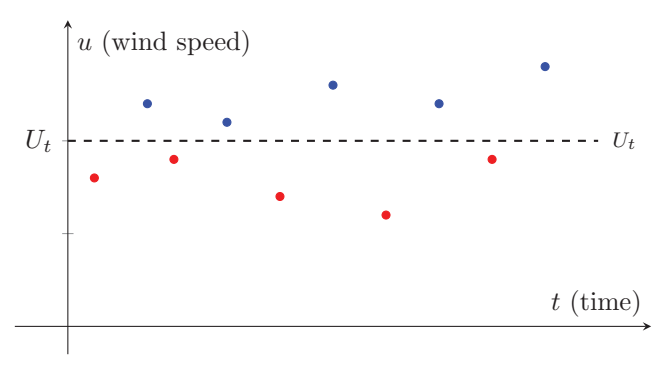


Figure 6: The plot shows the variation of wind speed (U) over time (t). The dashed black line represents the transport threshold speed. Points above the threshold $(U > U_t)$, shown in blue, indicate conditions where sediment transport is likely to occur. Points below or at the threshold $(U \le U_t)$, shown in red, indicate conditions where transport does not occur.

The onshore projected component of the transport rate can be estimated by:

$$|q_{s\perp}(t)| = |q_s(t)\sin\left(\theta(t)\right)|\Theta\left(\theta \in (0,\pi)\right) \tag{12}$$

Where $|q_{s\perp}(t)|$ denotes the projected component of the sediment transport rate at time t, $q_s(t)$ represents the sediment transport rate, $\theta(t)$ is the angle between the wind direction and the shoreline orientation, and $\Theta(\theta \in (0, \pi))$ ensures that sediment transport is only calculated when the transport direction is onshore.

To calculate the average sediment transport rate over a period T, we integrate the instantaneous sediment transport rate $|q_s(t)|$ over time, expressed as:

$$\overline{q} = \frac{1}{T} \int_0^T |q_s(t)| \, dt = \frac{1}{N} \sum_{i=1}^N |q_s(t_i)| \tag{13}$$

The average onshore projected component of the transport rate can be calculated by:

$$\overline{q_{\perp}} = \frac{1}{T} \int_0^T |q_{s\perp}(t)| \, dt = \frac{1}{N} \sum_{i=1}^N |q_{s\perp}(t_i)| \tag{14}$$

To apply the sediment transport model described above, we used wind data obtained from the San Bernard National Wildlife Refuge (NWR) weather station (28.864°N, 95.567°W), located approximately 7km from the monitoring site. The station lies well within the integral length scale for wind velocity, ensuring that the measurements are representative of the study area. Wind speed was recorded at a height of 14ft above ground level. Hourly average and maximum wind velocities were converted from miles per hour to meters per second. Wind directions were adjusted relative to the shoreline orientation (approximately 30°). Based on [3], we selected $3.5 \,\text{m/s}$ as the threshold wind speed (U_t) for initiating sediment transport. We also assumed that sand transport could occur during both day and night. To maintain compatibility with the referenced methodology, adjustments for Daylight Saving Time (DST) were excluded, and wind data—originally recorded in Greenwich Mean Time (GMT)—were converted to Central Standard Time (CST) to align with regional observations.

3.5 After-Storm Dune Recovery

Understanding how quickly dunes recover after storm events is essential for evaluating barrier island resilience. Our recent model [9] describes the competition between dune accretion driven by the wind and dune erosion driven by overtopping by high water events (HWEs). Dune growth is characterized by the maximum (averaged) growth rate G_d , whereas the frequency of HWEs is characterized by the mean size of HWEs, \overline{S} and the characteristic elevation of the barrier in the absence of a dune. We define this elevation of a dune-less barrier as the barrier's elevation capital h_c . Another interpretation of the elevation capital is as the characteristic elevation of the barrier following dune erosion after a large overwash.

In terms of these parameters, the model predicts that dunes will tend to recover whenever the local elevation capital is above the threshold:

$$h_{cc} = \overline{S} \left(\ln \left(\lambda_r \overline{S} / G_d \right) - 1 \right) \tag{15}$$

where $\lambda_r = 18 \text{yr}^{-1}$.

When the local elevation capital is above the critical one $(h_c > h_{cc})$, dunes should be able to naturally rebuild through wind-driven sediment transport and vegetation growth. However, if elevation capital is lower than this limit, even low-intensity high-water events can repeatedly inundate the surface, preventing dune reformation and leaving the barrier in a persistently vulnerable state.

This quantitative threshold for elevation capital thus define a tipping point between stable dune formation and chronic flooding conditions, allowing for better predictions of barrier island stability.

4 Site Description

This section presents an overview of the Cedar Lakes site, focusing on its coastal morphology and sediment dynamics. It is organized into two main parts: the first examines the spatial and temporal evolution of the barrier, dune, and beach systems using historical maps and elevation data; the second analyzes elevation change rates and sediment transport processes that influence barrier stability and recovery.

In what follows, all elevations will be relative to the characteristic beach elevation $Z_r = 1$ m.

4.1 Topographic data and Growth Rate Analysis

Figures 7 through 14 display detailed morphological maps for the available DEMs analyzed (Section 2.2).

The barrier width increased over time, primarily due to shoreline accretion. Initially, in 2001, the barrier was relatively narrow, with limited washover. By 2009, the washover region widened.

Originally, the site featured only a single primary dune system. However, following Hurricane Harvey and the resulting shoreline accretion, a secondary dune system developed, particularly prominent on the eastern side.

Consequently, three distinct morphological regions were identified across the barrier:

- West Side: Characterized by a poorly developed dune system.
- Washover Region: Lacked dunes due to consistent overwash activity.
- East Side: Exhibited well-developed dunes, providing greater stability.

Figures 15 to 21 show growth rate maps for the available DEMs analyzed (see Section 2.2). The growth rate maps also confirm shoreline accretion over time, with a marked increase in beach width following Hurricane Harvey. The washover region appeared as the most morphologically dynamic area—widening by 2009, narrowing by 2012, breaching again during Hurricane Harvey.

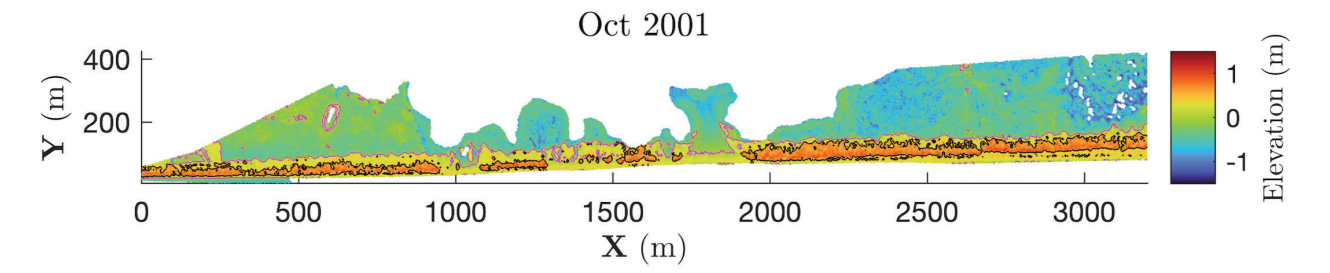


Figure 7: Map of the Cedar Lakes site from October 2001, showing key morphological features. The magenta line represents the 0 m contour (beach), while the black line indicates the 0.5 m contour (dune region). These contours provide insight into beach-dune interactions and the potential for overwash and dune recovery.

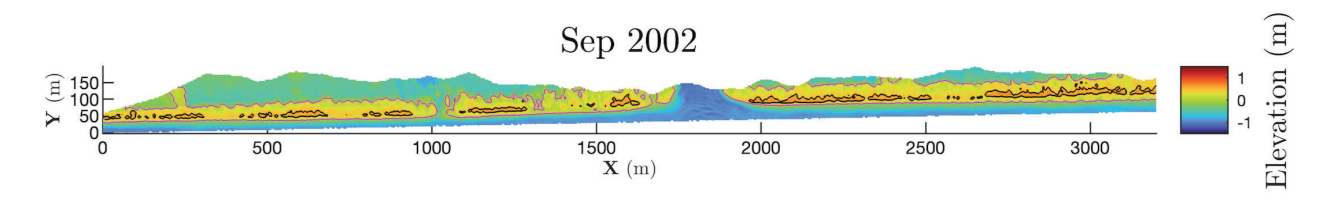


Figure 8: Map of the Cedar Lakes site from September 2002, showing key morphological features. The magenta line represents the 0 m contour (beach), while the black line indicates the 0.5 m contour (dune region). These contours provide insight into beach-dune interactions and the potential for overwash and dune recovery.

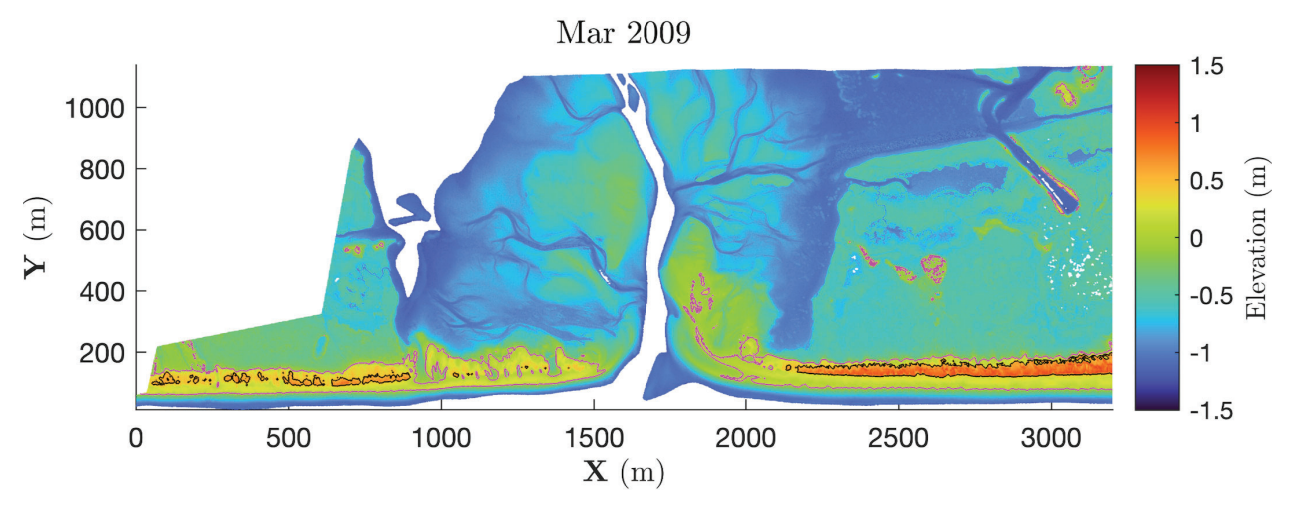


Figure 9: Map of the Cedar Lakes site from March 2009, showing key morphological features. The magenta line represents the 0 m contour (beach), while the black line indicates the 0.5 m contour (dune region). These contours provide insight into beach-dune interactions and the potential for overwash and dune recovery.

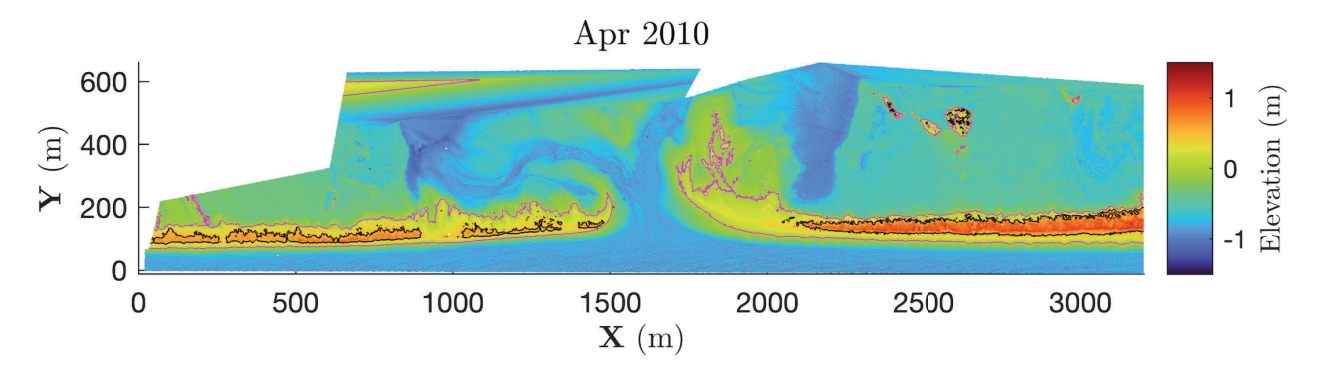


Figure 10: Map of the Cedar Lakes site from April 2010, showing key morphological features. The magenta line represents the 0 m contour (beach), while the black line indicates the 0.5 m contour (dune region). These contours provide insight into beach-dune interactions and the potential for overwash and dune recovery.

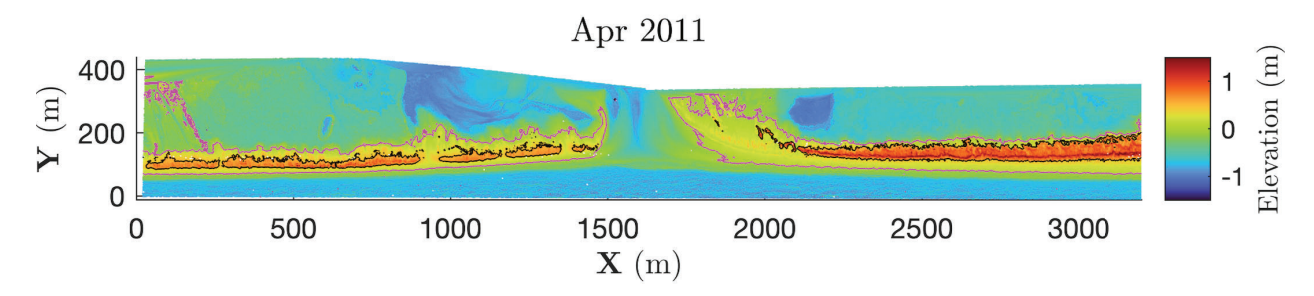


Figure 11: Map of the Cedar Lakes site from April 2011, showing key morphological features. The magenta line represents the 0 m contour (beach), while the black line indicates the 0.5 m contour (dune region). These contours provide insight into beach-dune interactions and the potential for overwash and dune recovery.

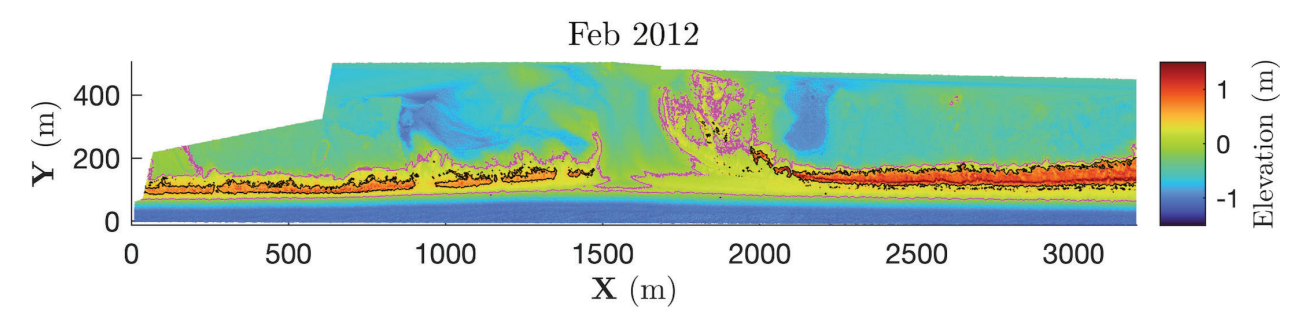


Figure 12: Map of the Cedar Lakes site from February 2012, showing key morphological features. The magenta line represents the 0 m contour (beach), while the black line indicates the 0.5 m contour (dune region). These contours provide insight into beach-dune interactions and the potential for overwash and dune recovery.

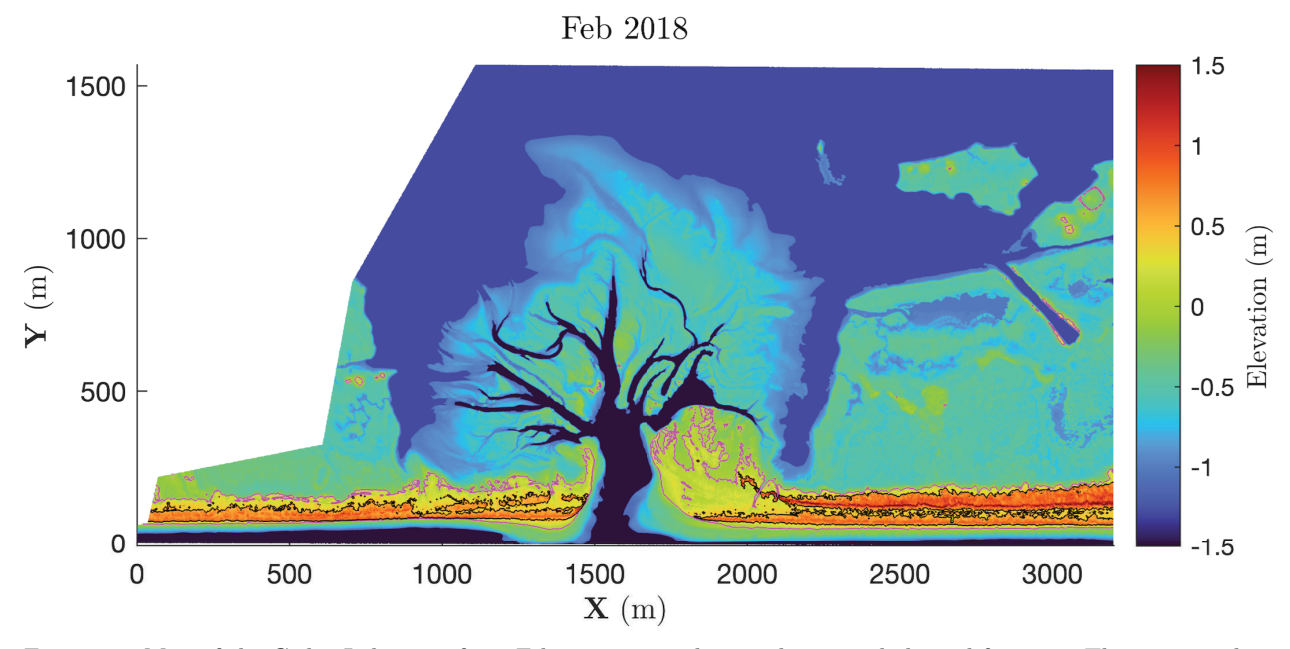


Figure 13: Map of the Cedar Lakes site from February 2018, showing key morphological features. The magenta line represents the 0 m contour (beach), while the black line indicates the 0.5 m contour (dune region). These contours provide insight into beach-dune interactions and the potential for overwash and dune recovery.

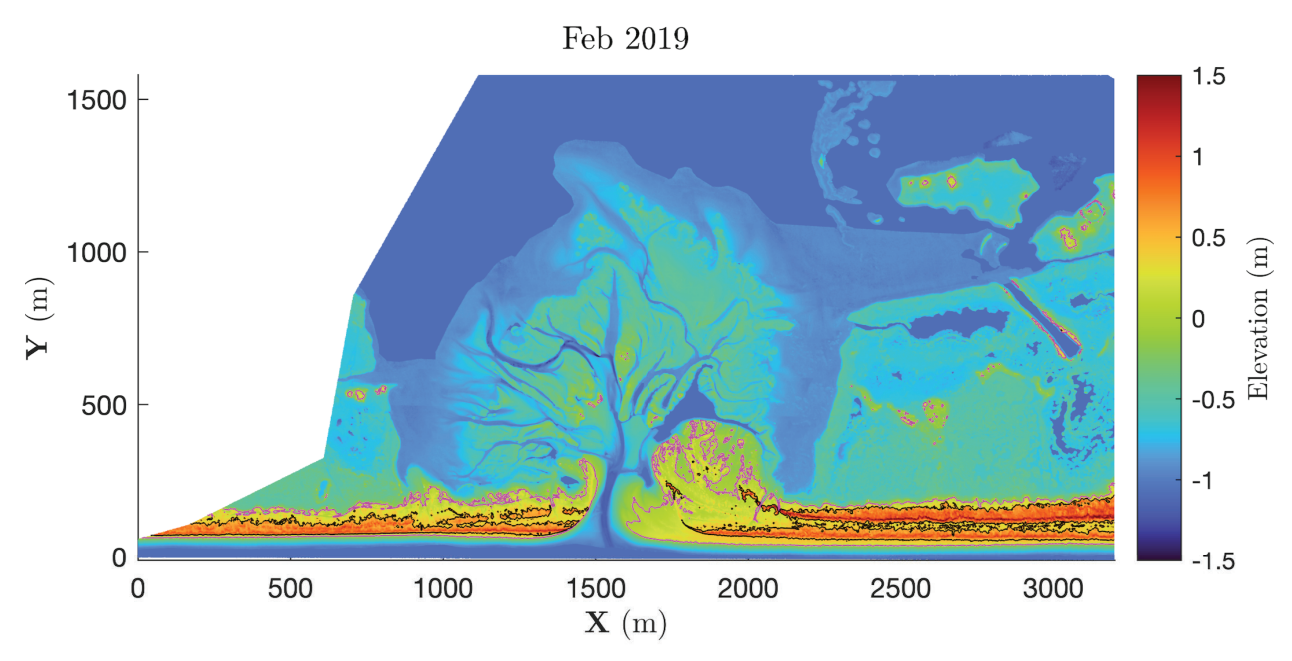


Figure 14: Map of the Cedar Lakes site from February 2019, showing key morphological features. The magenta line represents the 0 m contour (beach), while the black line indicates the 0.5 m contour (dune region). These contours provide insight into beach-dune interactions and the potential for overwash and dune recovery.

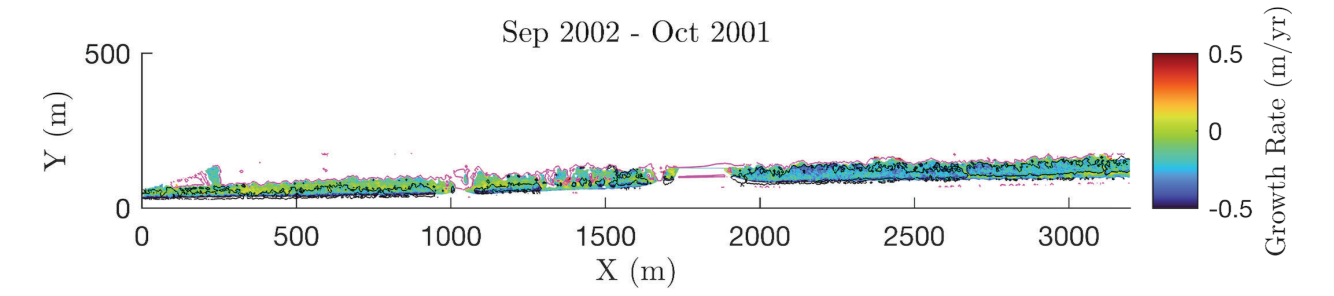


Figure 15: Growth rate map of the Cedar Lakes site between October 2001 and September 2002. The magenta line represents the 0 m contour (beach), while the black line indicates the 0.5 m contour (dune region). This figure highlights elevation changes and sediment redistribution, providing insights into the short-term morphological evolution of the site.

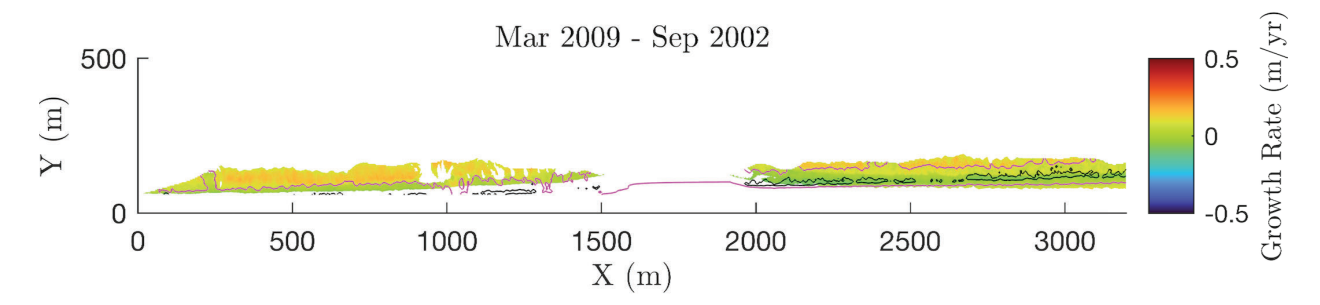


Figure 16: Growth rate map of the Cedar Lakes site between September 2002 and March 2009. The magenta line represents the 0 m contour (beach), while the black line indicates the 0.5 m contour (dune region). This figure highlights elevation changes and sediment redistribution, providing insights into the short-term morphological evolution of the site.

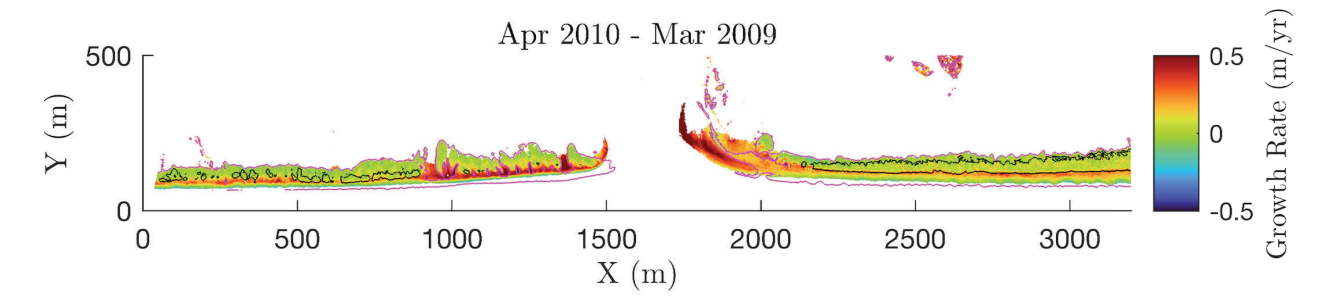


Figure 17: Growth rate map of the Cedar Lakes site between March 2009 and April 2010. The magenta line represents the 0 m contour (beach), while the black line indicates the 0.5 m contour (dune region). This figure highlights elevation changes and sediment redistribution, providing insights into the short-term morphological evolution of the site.

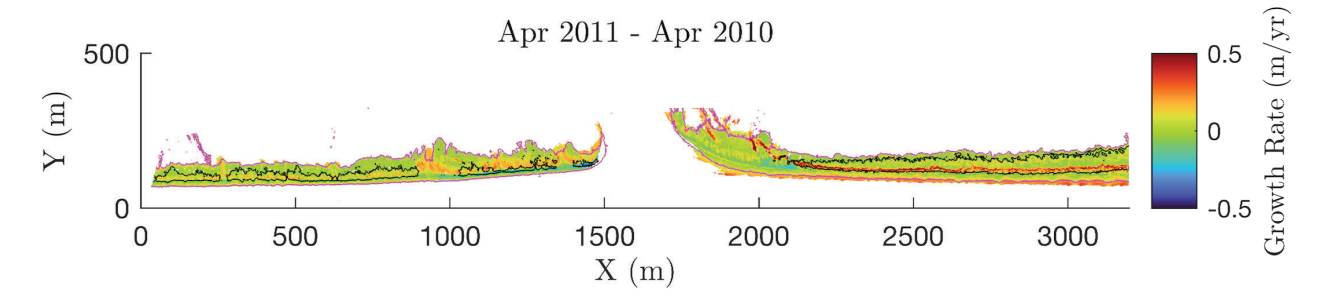


Figure 18: Growth rate map of the Cedar Lakes site between April 2010 and April 2011. The magenta line represents the 0 m contour (beach), while the black line indicates the 0.5 m contour (dune region). This figure highlights elevation changes and sediment redistribution, providing insights into the short-term morphological evolution of the site.

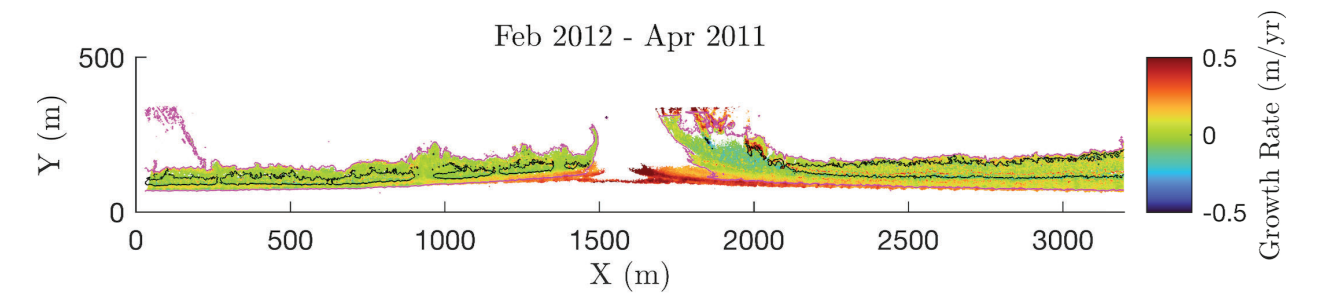


Figure 19: Growth rate map of the Cedar Lakes site between April 2011 and February 2012. The magenta line represents the 0 m contour (beach), while the black line indicates the 0.5 m contour (dune region). This figure highlights elevation changes and sediment redistribution, providing insights into the short-term morphological evolution of the site.

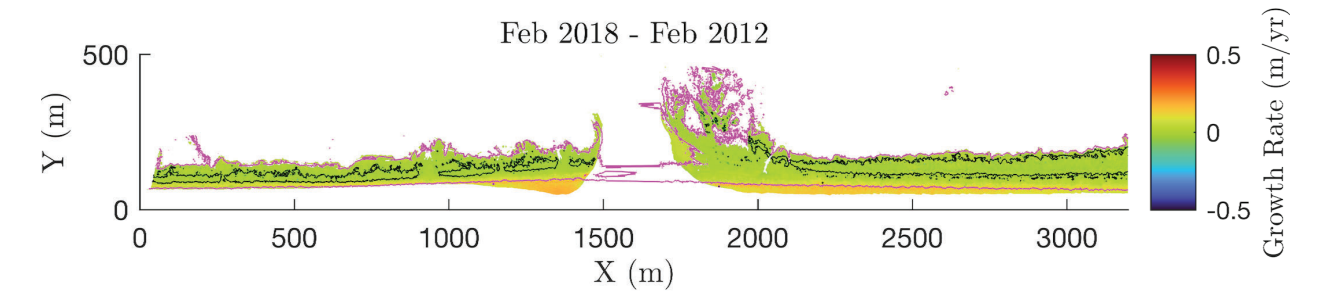


Figure 20: Growth rate map of the Cedar Lakes site between February 2012 and February 2018. The magenta line represents the 0 m contour (beach), while the black line indicates the 0.5 m contour (dune region). This figure highlights elevation changes and sediment redistribution, providing insights into the short-term morphological evolution of the site.

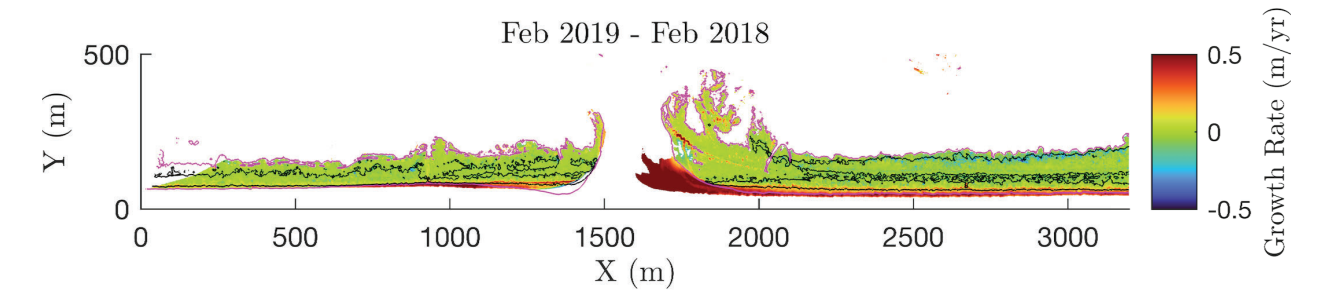


Figure 21: Growth rate map of the Cedar Lakes site between February 2018 and February 2019. The magenta line represents the 0 m contour (beach), while the black line indicates the 0.5 m contour (dune region). This figure highlights elevation changes and sediment redistribution, providing insights into the short-term morphological evolution of the site.

4.2 Morphological Characteristics

This section provides a detailed examination of the morphological characteristics of the Cedar Lakes site, focusing on barrier and dune evolution from March 2009 to February 2019. It begins by presenting barrier morphological metrics, including temporal changes in barrier height and width. The evolution of dune morphology is subsequently addressed, highlighting variations in dune heights, widths, and aspect ratios.

4.2.1 Barrier Characteristics

This section analyzes barrier morphology at the Cedar Lakes site from March 2009 to February 2019, with a focus on changes in barrier height and width. All elevation values are reported relative to the beach reference elevation (see Section 3.2).

Temporal variations in barrier height are shown in Figures 22 and Table 2. The barrier height increased between 2009 and 2012 but declined afterward, primarily due to the impacts of Hurricane Harvey. By 2019, the barrier exhibited signs of recovery, with a noticeable increase in height. Specifically, the average barrier height rose from 0.7 m in 2009 to 1.1 m in 2019. Across the site, average primary dune heights ranged between 0.7 and 1.0 m.

The dune height distribution revealed two distinct modes, indicating the presence of morphologically different regions. The west side featured a poorly developed dune system, while the east side had well-developed dunes that contributed to greater barrier stability. The modal dune heights were approximately 0.6 m on the west side and 0.9 m on the east side, corresponding to the lower and upper peaks in the distribution plot. By 2012, these modal dune heights increased to 0.7 m and 1.3 m, respectively.

Figures 23 and Table 3 present the evolution of barrier width over the study period. The results highlight phases of beach accretion that contributed to the overall increase in barrier width from 2009 to 2019. Notably, the barrier expanded from 90 meters in 2009 to 120 meters in 2019, with much of this growth attributed to shoreline accretion following Hurricane Harvey.

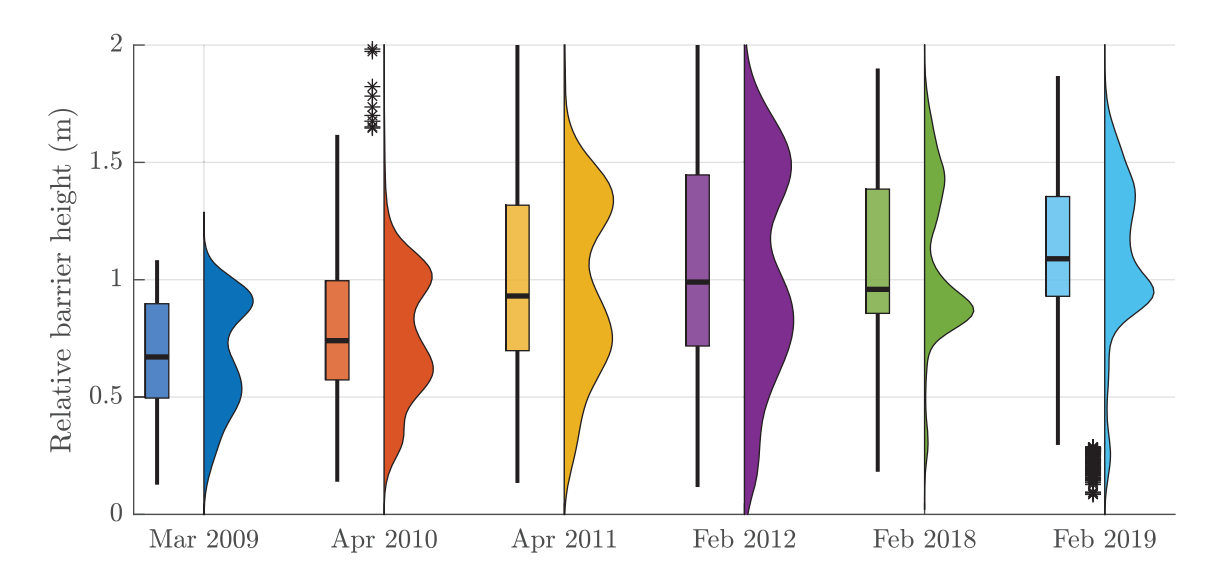


Figure 22: Temporal evolution of barrier height at the Cedar Lakes site from March 2009 to February 2019, relative to the beach. The barrier height increased from March 2009 to February 2012, followed by a decline in February 2018, likely due to storm-induced erosion. In February 2019, barrier height increased again, suggesting post-storm recovery. The presence of two peaks in some years suggests distinct elevation distributions between the eastern and western sections of the barrier, with the eastern region generally exhibiting higher elevations than the western region.

Table 2: Summary statistics for the barrier height (m) distribution relative to the beach: the mode (H_{Mode}) , the mean (H_{Mean}) , the 75th percentile (H_{75}) , the 90th percentile (H_{90}) , and the maximum value (H_{max}) .

Year	$H_{ m Mode}$	$H_{ m Mean}$	H_{75}	H_{90}	$H_{ m max}$
Mar 2009	0.9	0.7	0.9	1.0	1.1
Apr 2010	1.0	0.8	1.0	1.1	1.6
Apr 2011	1.3	1.0	1.3	1.4	2.2
Feb 2012	1.5	1.0	1.4	1.6	2.2
Feb 2018	1.4	1.1	1.4	1.5	1.9
Feb 2019	1.3	1.1	1.4	1.5	1.9

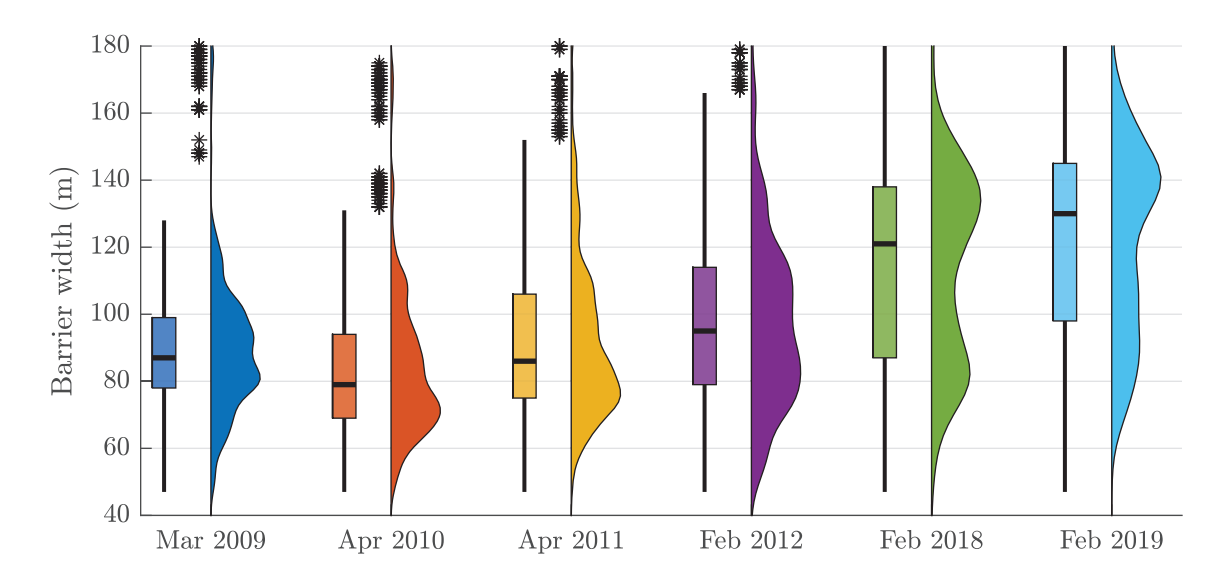


Figure 23: Temporal evolution of barrier width at the Cedar Lakes site from March 2009 to February 2019. During this period, the barrier width increased due to beach accretion.

Table 3: Summary statistics for the barrier width (m) distribution: the mode (W_{Mode}) , the mean (W_{Mean}) , the 75th percentile (W_{75}) , the 90th percentile (W_{90}) , and the maximum value (W_{max}) .

Year	$W_{ m Mode}$	$W_{ m Mean}$	W_{75}	W_{90}	$W_{\rm max}$
Mar 2009	92	88	98	108	128
Apr 2010	106	81	92	107	131
Apr 2011	106	90	103	122	152
Feb 2012	108	97	113	131	166
Feb 2018	134	117	138	149	214
Feb 2019	140	123	144	157	215

4.2.2 Dune Morphological Evolution

This section provides a detailed analysis of the morphological evolution of dunes at the Cedar Lakes site from March 2009 to February 2019, focusing on dune height, dune width, and aspect ratios. All elevations reported are relative to the beach reference elevation (see Section 3.2).

Figure 24 and Table 4 illustrate temporal changes in dune heights. Average primary dune heights across the site generally ranged from 0.8 to 1.0 m.

Figure 25 and Table 5 show the evolution of primary dune widths. The dune widths remained relatively

stable over time, consistently falling between 20 and $30\,\mathrm{m}$.

Finally, Figure 26 and Table 6 present the aspect ratios of the dunes, defined as the ratio of dune height to width. These aspect ratios ranged from 0.02 to 0.04 throughout the analysis period.

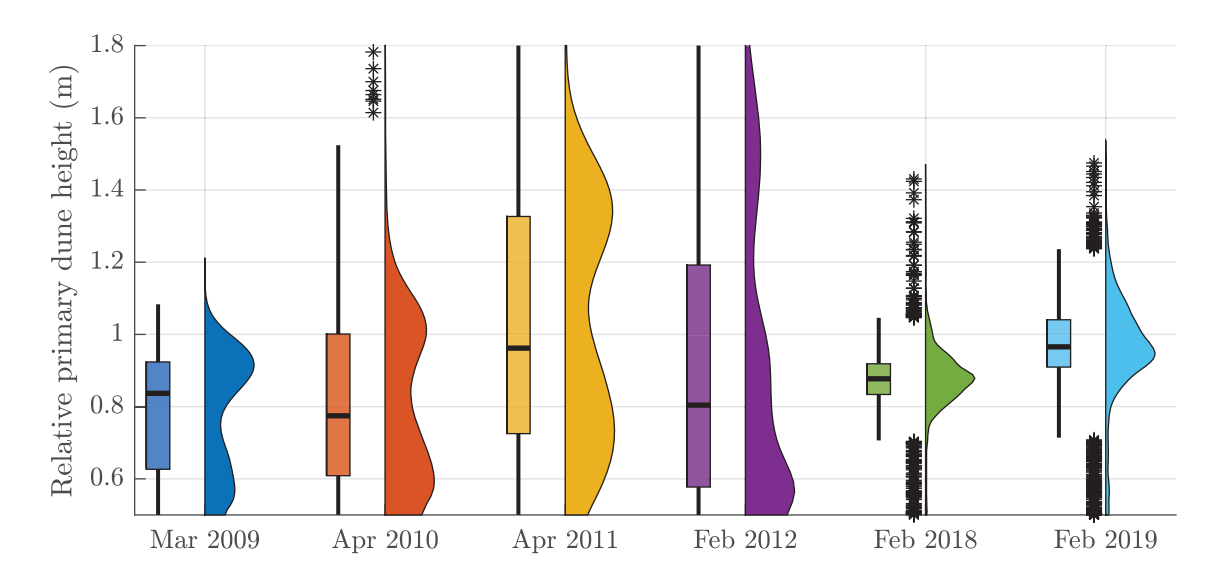


Figure 24: Temporal evolution of dune heights relative to the beach at the Cedar Lakes site from March 2009 to February 2019.

Table 4: Summary statistics for the dune height (m) distribution relative to the beach: the mode (H_{Mode}) , the mean (H_{Mean}) , the 75th percentile (H_{75}) , the 90th percentile (H_{90}) , and the maximum value (H_{max}) .

Year	$H_{ m Mode}$	$H_{ m Mean}$	H_{75}	H_{90}	$H_{ m max}$
Mar 2009	0.9	0.8	0.9	1.0	1.1
Apr 2010	1.0	0.8	1.0	1.1	1.5
Apr 2011	1.3	1.0	1.3	1.4	2.2
Feb 2012	1.5	0.9	1.2	1.5	2.1
Feb 2018	0.9	0.9	0.9	1.0	1.0
Feb 2019	0.9	1.0	1.0	1.1	1.2

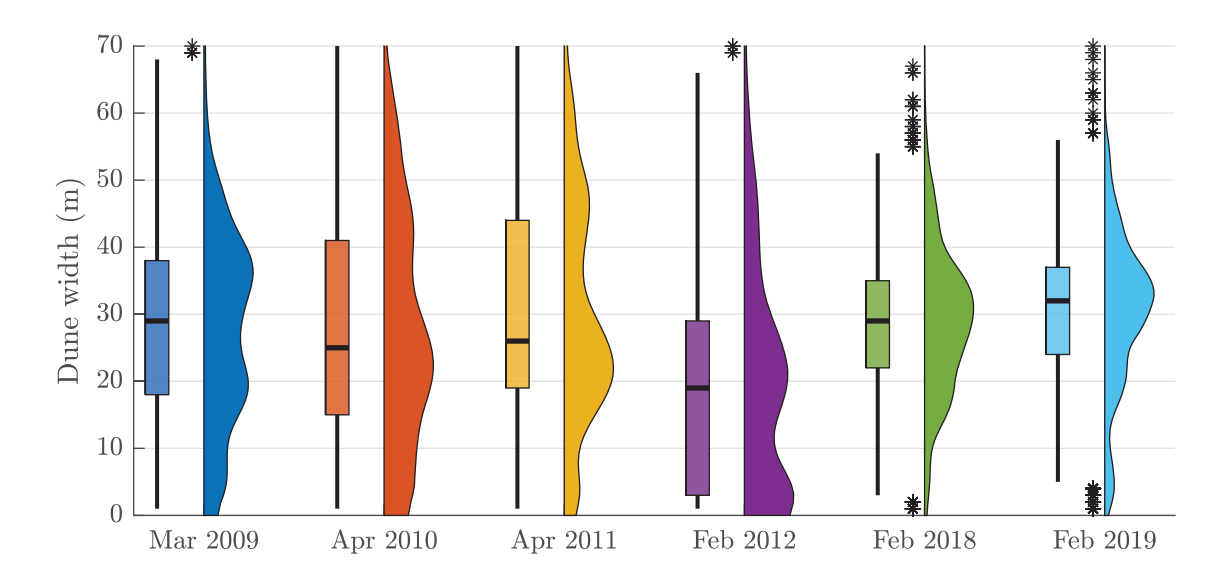


Figure 25: Temporal evolution of dune widths at the Cedar Lakes site from March 2009 to February 2019.

Table 5: Summary statistics for the dune width (m) distribution: the mode (W_{Mode}) , the mean (W_{Mean}) , the 75th percentile (W_{75}) , the 90th percentile (W_{90}) , and the maximum value (W_{max}) .

Year	$W_{ m Mode}$	$W_{ m Mean}$	W_{75}	W_{90}	$W_{ m max}$
Mar 2009	36	28	38	46	68
Apr 2010	42	28	41	52	80
Apr 2011	45	30	44	54	81
Feb 2012	21	19	28	44	66
Feb 2018	31	29	35	42	54
Feb 2019	33	31	37	44	56

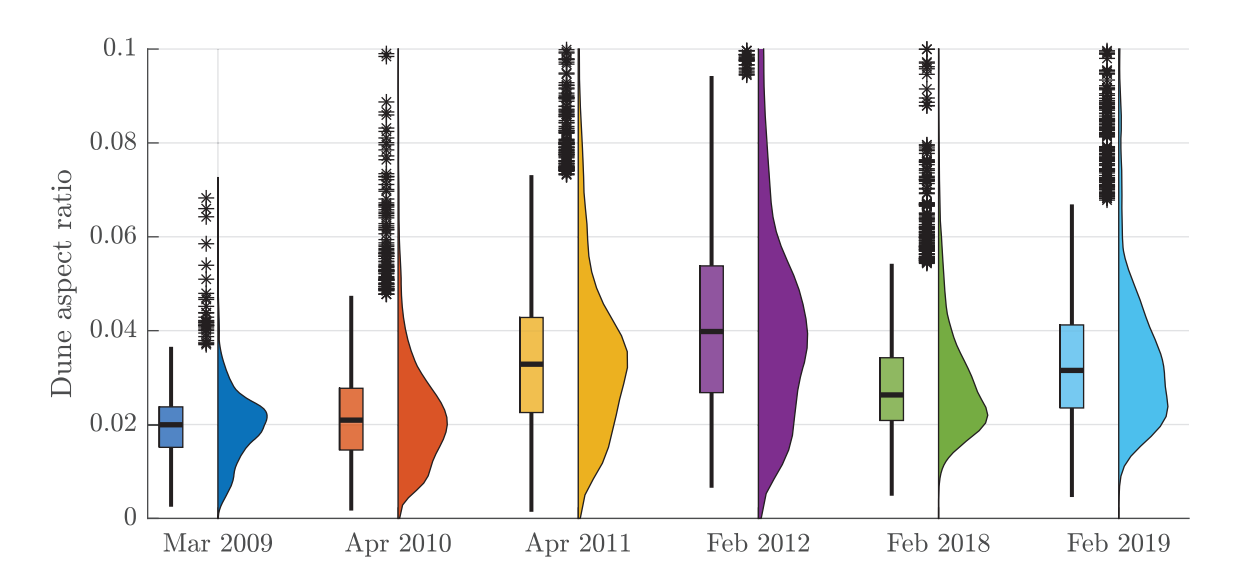


Figure 26: Temporal evolution of dune aspect ratios at the Cedar Lakes site from March 2009 to February 2019. The aspect ratio is defined as the ratio of dune height to width.

Table 6: Summary statistics for the dune aspect ratio distribution: the mode (A_{Mode}) , the mean (A_{Mean}) , the 75th percentile (A_{75}) , the 90th percentile (A_{90}) , and the maximum value (A_{max}) .

Year	$A_{ m Mode}$	$A_{ m Mean}$	A_{75}	A_{90}	A_{\max}
Mar 2009	0.022	0.019	0.024	0.027	0.037
Apr 2010	0.020	0.021	0.027	0.033	0.047
Apr 2011	0.034	0.032	0.041	0.052	0.073
Feb 2012	0.038	0.040	0.051	0.068	0.094
Feb 2018	0.022	0.027	0.033	0.041	0.054
Feb 2019	0.024	0.032	0.039	0.047	0.067

4.2.3 Evolution of the Length of the Dry Beach and Relation to Dune Size

Based on the definition of the characteristic beach elevation (Z_r) , we define the potential length of the dry-sand beach as the distance from the location with elevation Z_r and the dune crest heretofore referred as beach-to-dune crest distance. This length thus provide an estimation of potential sand supply driven by wind transport to form dunes.

Figure 27 shows the alongshore variation in beach-to-dune crest distance computed using a 100-meter moving average, highlighting the evolution and spatial heterogeneity in beach width relative to dune positions over the study period. Figure 28 further illustrates the distribution of beach-to-dune crest distances, emphasizing

the variability and providing insight into patterns of sediment deposition and erosion processes along the shoreline.

Figure 29 presents a two-dimensional histogram that captures the relationship between dune height and beach-to-dune crest distances. This visualization reveals that taller dunes generally correspond with larger beach-to-dune crest distances, suggesting a strong interaction between dune growth, sediment availability, and transport dynamics. The theoretical upper bound of dune height (indicated by the red line in the figure) provides a reference framework to interpret observed dune sizes.

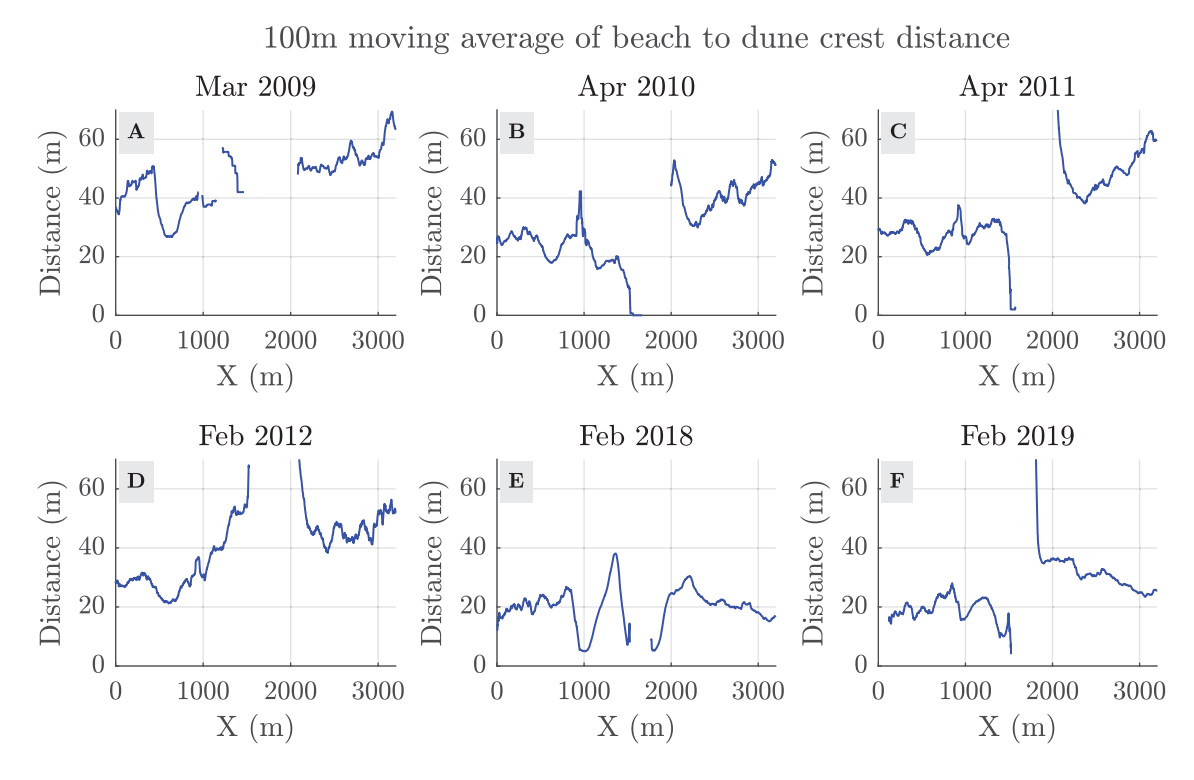


Figure 27: Temporal evolution of the alongshore beach-to-dune crest distance at the Cedar Lakes site, computed using a 100-meter moving average.

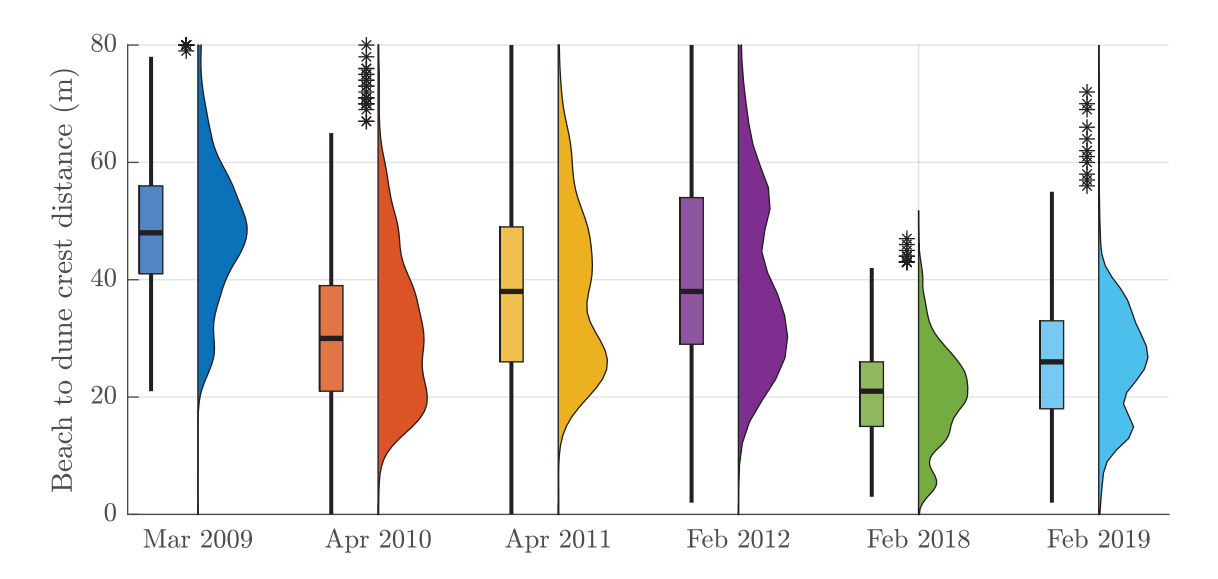


Figure 28: Distribution of beach-to-dune crest distances at the Cedar Lakes site.

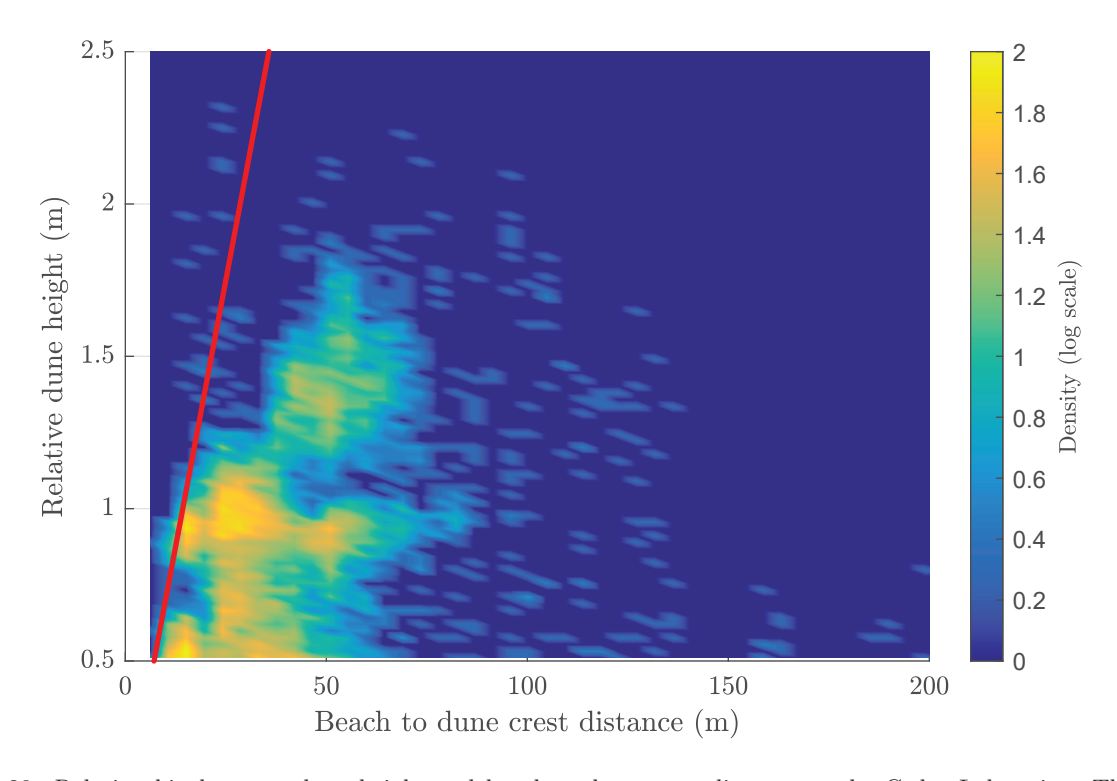


Figure 29: Relationship between dune height and beach-to-dune crest distance at the Cedar Lakes site. The 2D histogram illustrates a trend where taller dunes are generally associated with greater beach-to-dune crest distances, suggesting a linkage between dune formation processes and sediment transport dynamics. The red line represents the upper bound of dune height predicted by [1].

4.3 Sediment Budget and Elevation Change Rates

This section analyzes changes in beach and dune morphology by examining elevation growth rates and sediment volume change rates over time.

4.3.1 Elevation Change Rates

Figures 30 present temporal variations in alongshore growth rates for maximum elevation, barrier height, and dune crest, using 100-meter alongshore moving averages. Observed growth rates range from -0.5 to $0.5 \,\mathrm{m/yr}$.

Figure 31 and Table 7 show the relationship between initial elevation and the maximum elevation growth rate. On average, dunes grew at a rate of approximately $0.2 \,\mathrm{m/yr}$ over the study period. However, newly formed dunes exhibited substantially higher growth rates, reaching up to $0.9 \,\mathrm{m/yr}$ following Hurricane Harvey.

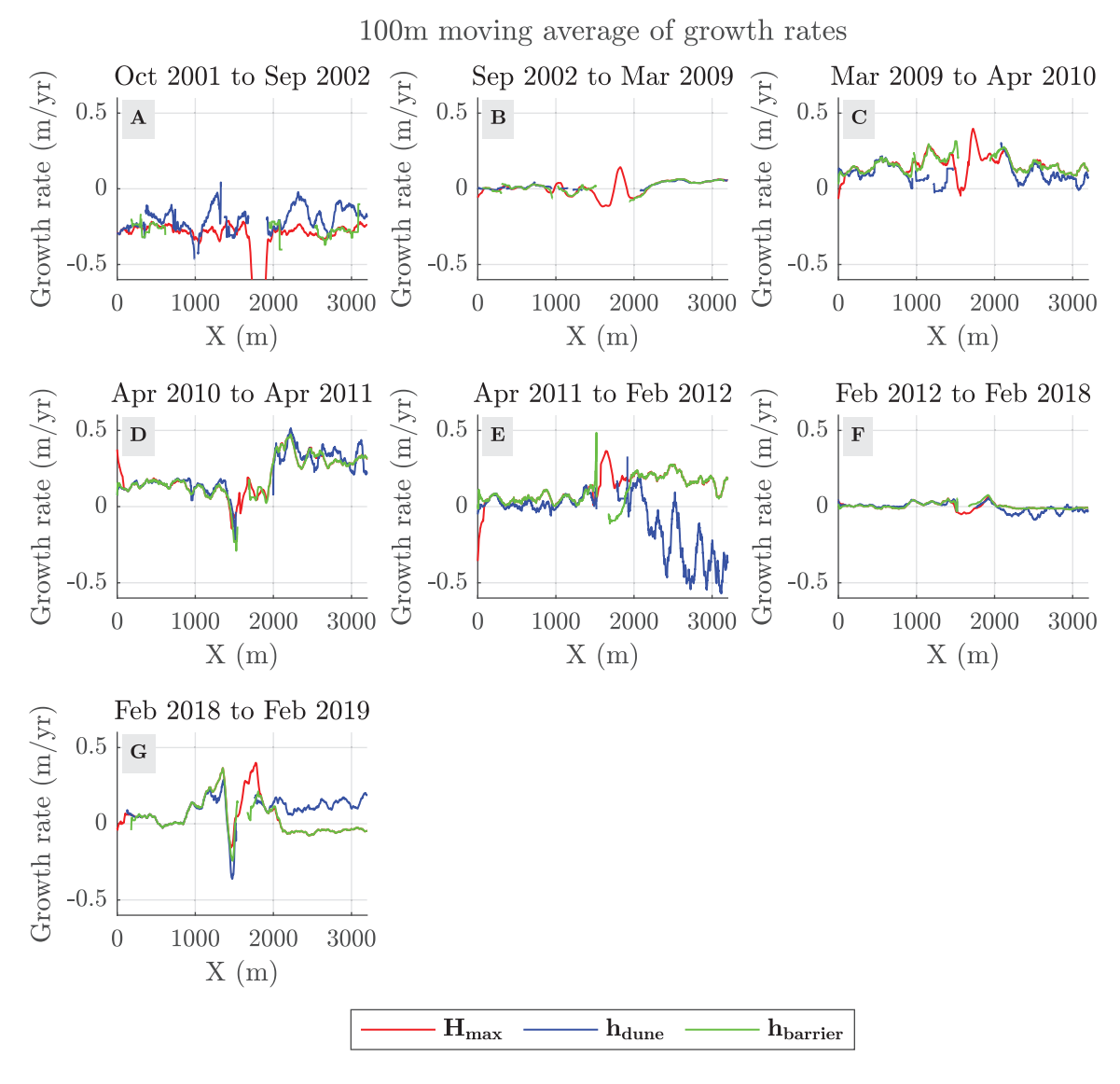


Figure 30: Alongshore growth rates averaged over a 100-meter moving window for consecutive intervals. The red line represents the growth rate of maximum elevation, the blue line indicates the growth rate of dune crest elevation, and the green line shows the growth rate of barrier height (see Section 3.1 for definitions of each morphological characteristic). Growth rates range from -0.5 to $0.5 \,\mathrm{m/yr}$. Between 2001 and 2002, maximum elevation decreased, followed by a relatively stable period from 2002 to 2009. From 2009 to 2012, maximum elevations increased and washover regions became narrower. During Hurricane Harvey, the washover region widened again, followed by a recovery phase in which it narrowed. From 2018 to 2019, elevations increased on both the western and eastern sides of the barrier.

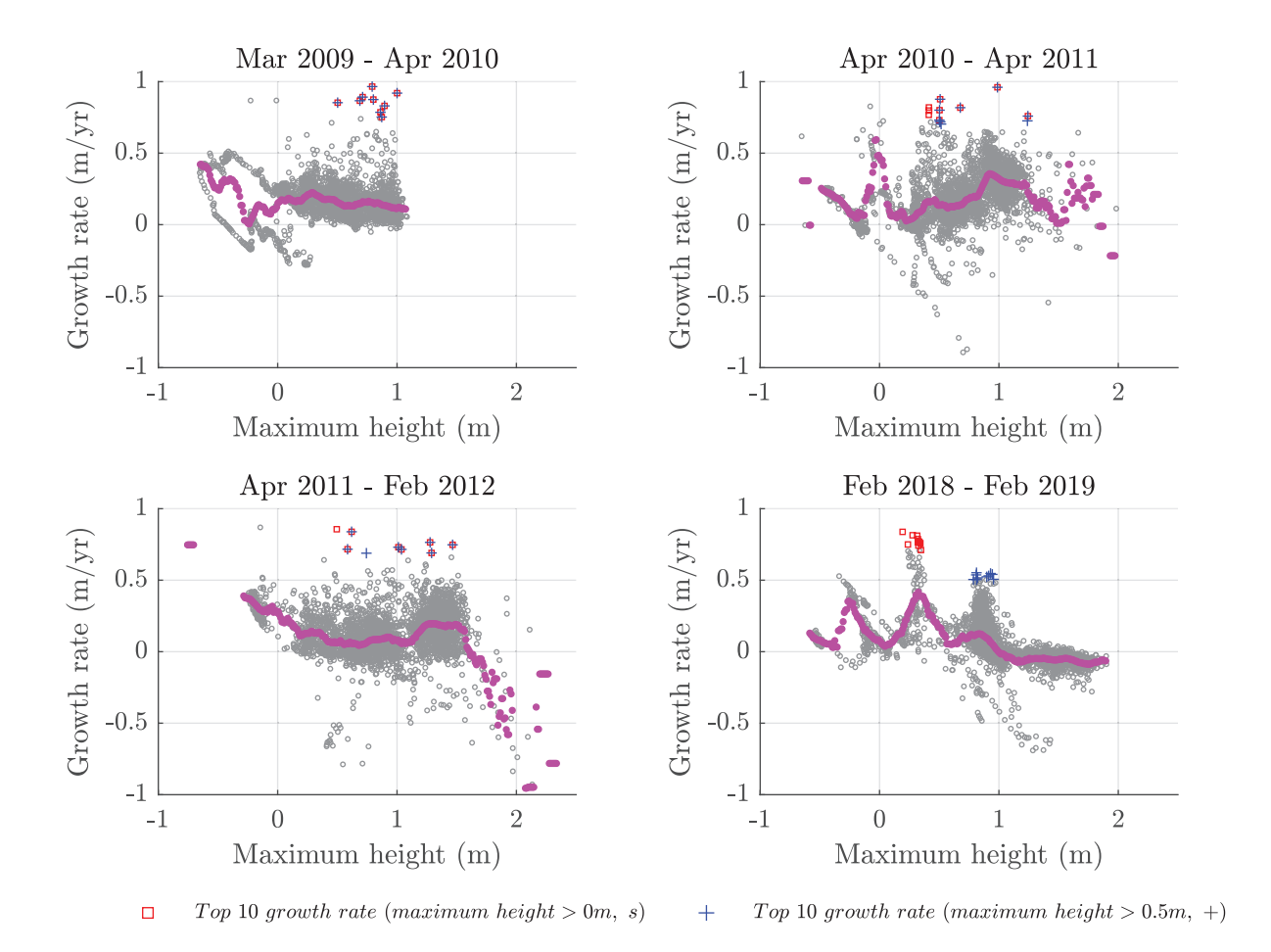


Figure 31: Relationship between the rate of maximum elevation change (m/yr) and initial elevation at different alongshore locations, relative to the reference beach elevation (see Section 3.2). Individual observations are shown as grey dots, with the average rate for a given initial elevation is shown by the magenta lines. Highlighted points represent the top 10 growth rates observed under two specific conditions: initial elevations above 0 m (beach level; primarily influenced by water-driven processes, red squares) and initial elevations above 0.5 m (dune base; primarily influenced by wind-driven processes, blue plus signs).

Table 7: Average and top 10 average growth rates of maximum elevation change (m/yr), based on the highlighted points in Figure 31. The first column shows the average growth rate for locations where the initial elevation ranged between 0.5 and 1 m above the reference beach elevation (see Section 3.2). The second column presents the top 10 average growth rates for locations with initial elevations greater than 0 m (beach level; primarily influenced by water-driven processes). The third column shows the top 10 average growth rates for locations with initial elevations exceeding 0.5 m (dune base; primarily influenced by wind-driven processes.

Period	Avg. Growth Rate (Initial Elevation Between $0.5-1 \text{ m}$) (m/yr)	Top 10 Avg. Growth Rate (Initial Elevation > 0 m) (m/yr)	Top 10 Avg. Growth Rate (Initial Elevation $> 0.5 \text{ m}$) (m/yr)
Mar 2009 to Apr 2010	0.14	0.88	0.88
Apr 2010 to Apr 2011	0.20	0.93	0.78
Apr 2011 to Feb 2012	0.07	0.82	0.80
Feb 2018 to Feb 2019	0.10	0.78	0.53

4.3.2 Beach and Dune Sediment Budget

Sediment volume change rate refers to the amount of sediment added to or removed from a specific location over a given time period, typically expressed as volume per unit shoreline length per unit time $(m^3/m/yr)$. For each cross-shore profile, sediment volume per unit shoreline length was calculated from the shoreline to the center of the barrier. Changes were determined by subtracting volumes between consecutive time intervals. The center of the barrier was selected as the landward boundary because it represents the transition from active beach processes to more stable back-barrier environments. This location generally remains unchanged over short timescales, providing a consistent reference point for comparison.

Figure 32 illustrates the spatial distribution of sediment volume change rates across consecutive time intervals, while Figure 33 shows the temporal distribution of these rates from March 2009 to February 2019. Sediment volume change rates ranged from approximately -10 to $10 \,\mathrm{m}^2/\mathrm{yr}$. Following Hurricane Harvey, the beach exhibited recovery at a rate consistent with the transport rate of $12.5 \,\mathrm{m}^2/\mathrm{yr}$, estimated for the same period using Equation 14, based on a wind speed threshold of $3.5 \,\mathrm{m/s}$ (see Section 5.3).

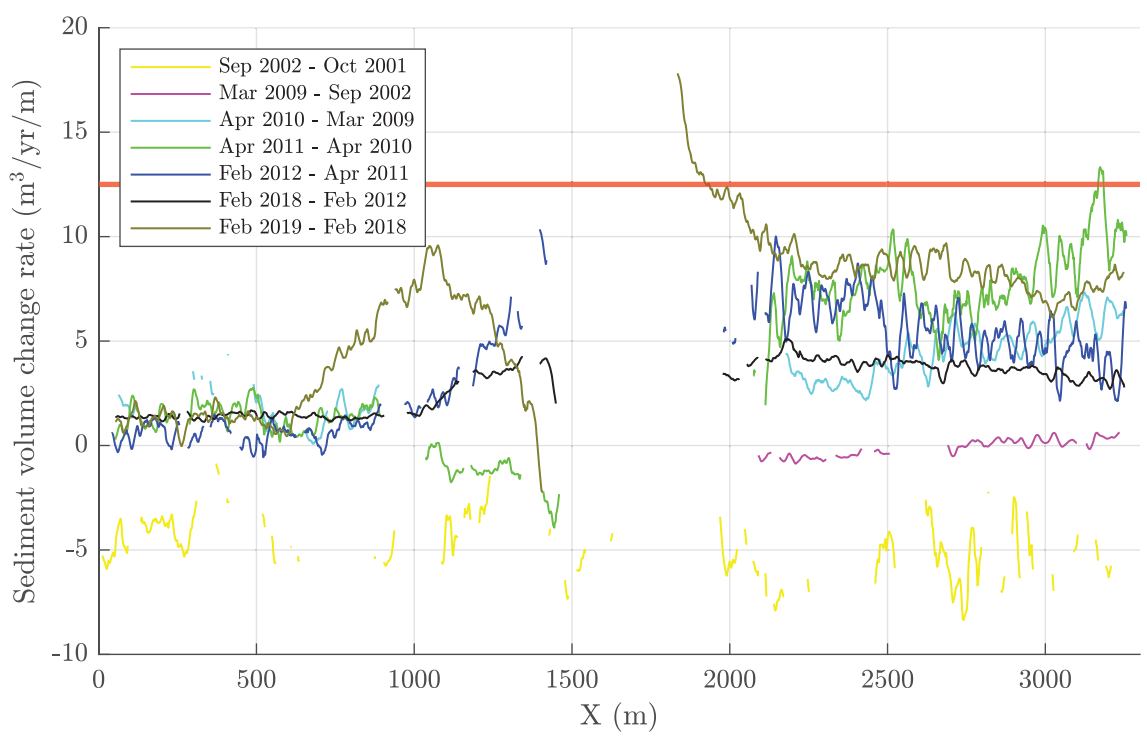


Figure 32: Comparison of sediment volume change rates across consecutive time intervals. Rates were calculated for each cross-shore profile from the shoreline to the center of the barrier. The red horizontal line represents the average on shore-projected sediment transport rate of $12.5 \text{ m}^2/\text{yr}$, calculated using Equation 14 for a wind speed threshold of 3.5 m/s (see Section 5.3). Following Hurricane Harvey, the beach recovered at a rate consistent with the transport rate estimated for the same period.

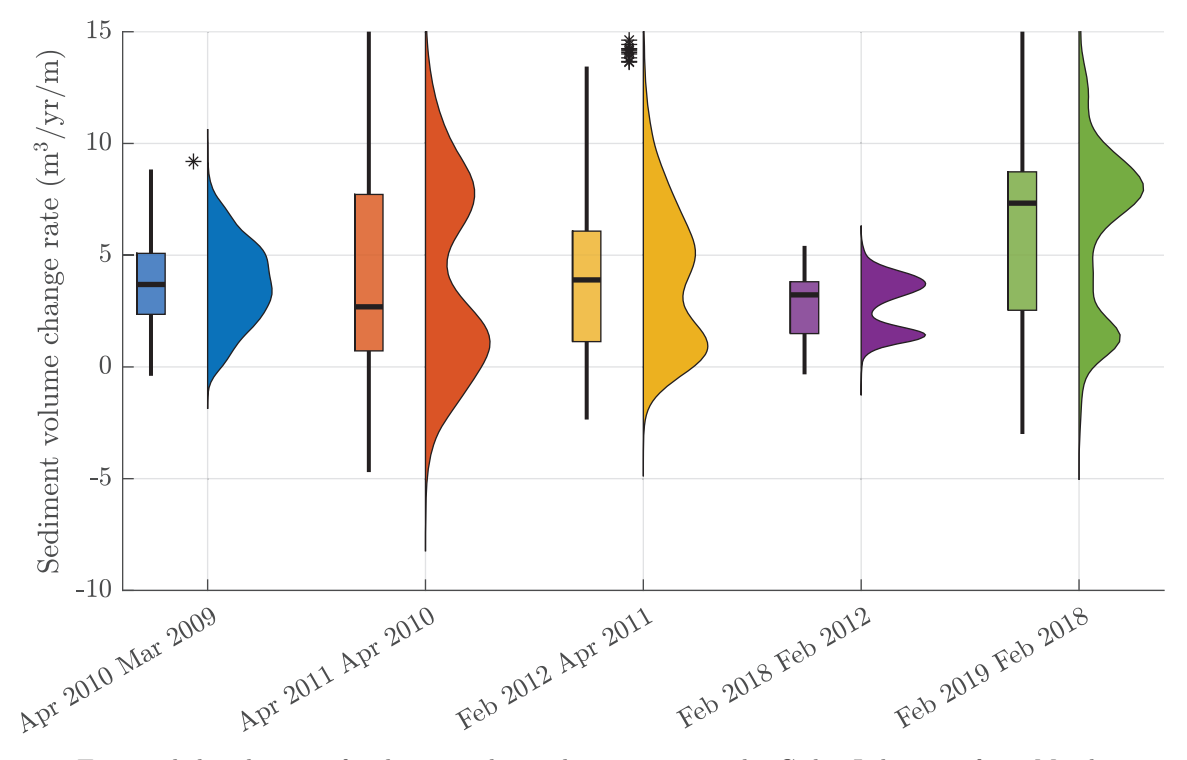


Figure 33: Temporal distribution of sediment volume change rates at the Cedar Lakes site from March 2009 to February 2019.

5 Model Prediction

5.1 High-Water Event (HWE) flooding

Although TWL time series were calculated for multiple offshore stations, we focused exclusively on Station 42002 (see Table 1) for this analysis because it provides the longest and most consistent dataset, making it well-suited for evaluating long-term trends and exceedance frequencies. All water level values presented in this section are referenced to MSL.

The daily maximum TWL ranged from 0 to 1.5 m, while the yearly maximum TWL ranged from about 0.5 to 4 m (see Figure 34).

In terms of potential flooding and dune erosion frequency, the daily maximum TWL exceeded 1 m every month. The dune recovery threshold (1.25 m; see Section 5.4) was exceeded every two months, while the dune base elevation (1.5 m; see Section 3.1) experienced flooding every four months. Additionally, TWL values exceeded 2 m annually and reached 2.7 m once every ten years (see Figure 36 and Table 8).

Figure 37 shows the proportion of days on which the TWL exceeded selected thresholds. The washover region was submerged approximately 10% of the time, whereas dunes with elevations above the average dune height (1.9 m; see Section 4.2.2) were submerged only about 0.1% of the time.

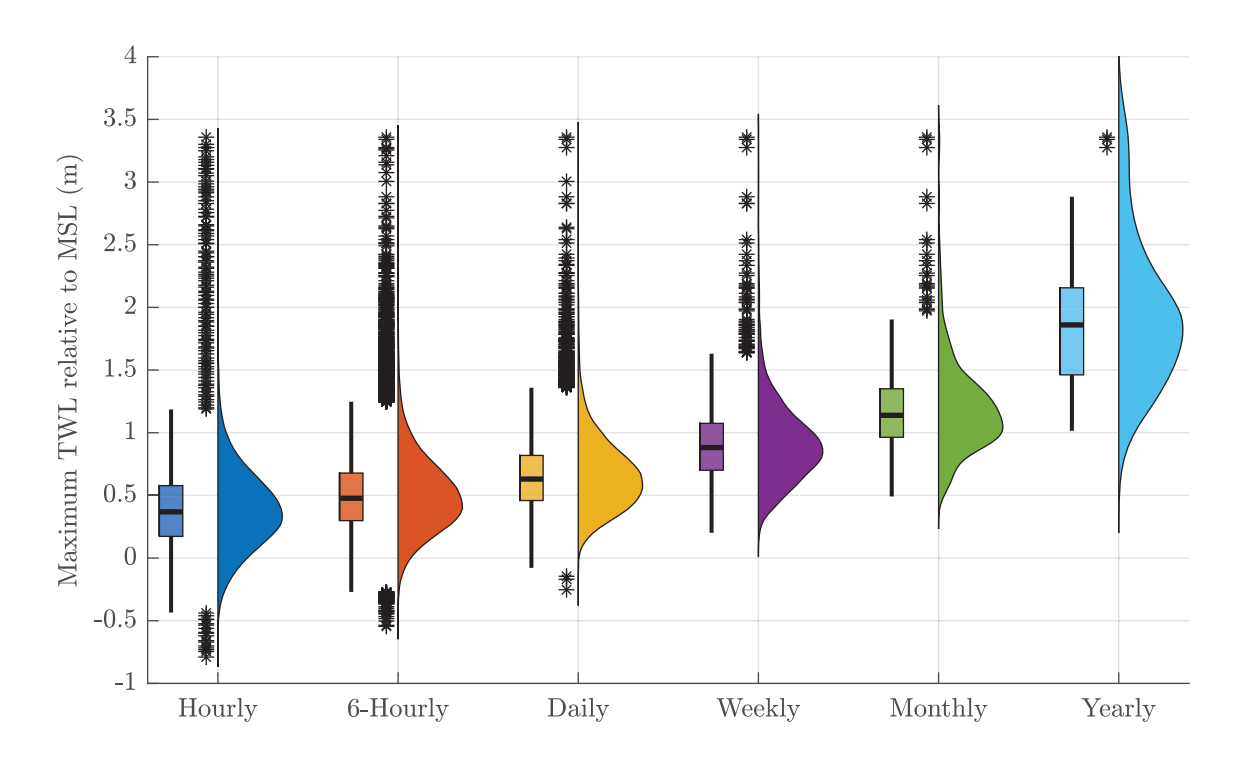


Figure 34: Distribution of TWL at the station 42002 for different time intervals.

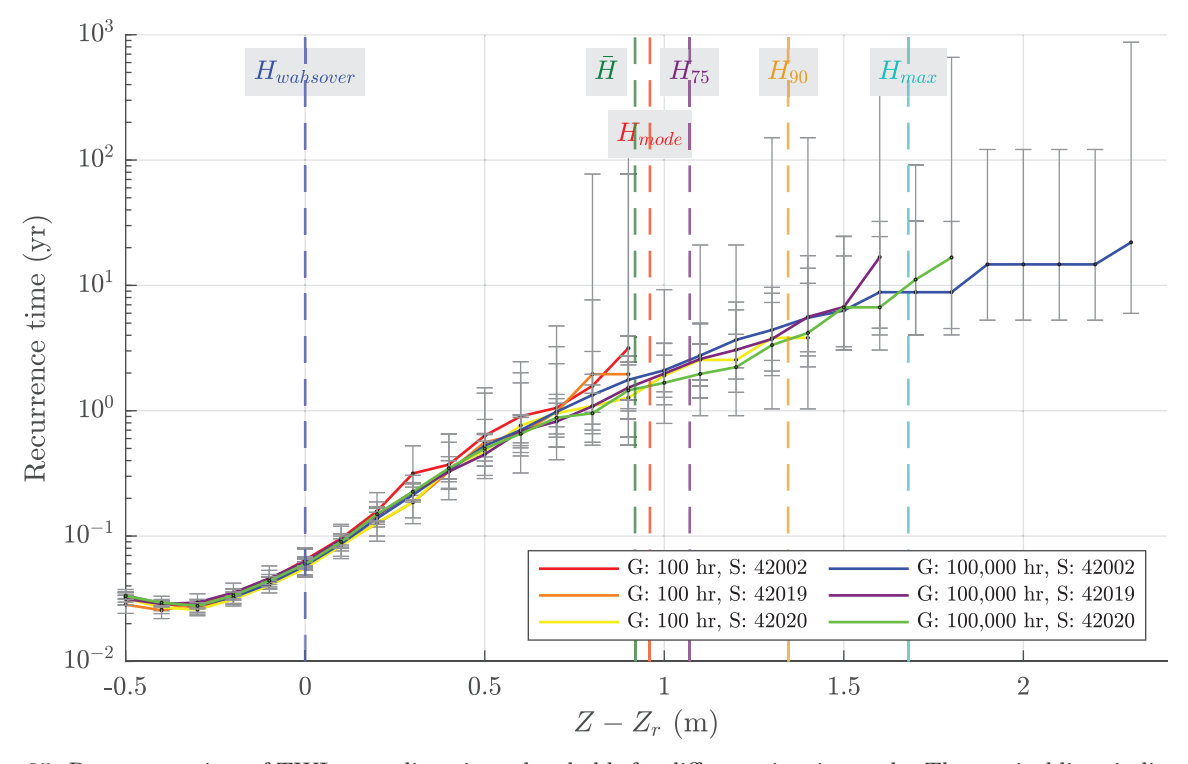


Figure 35: Recurrence time of TWL exceeding given thresholds for different time intervals. The vertical lines indicate key dune metrics: the mode (H_{Mode}) , the mean (H_{Mean}) , the 90th percentile (H_{90}) , the 75th percentile (H_{75}) , and the maximum dune height (H_{max}) (see Table 4 and Section 3.1). Different markers represent analyses from different wave stations (S) with varying data gaps (G) (see Table 1 and Section 3.2).

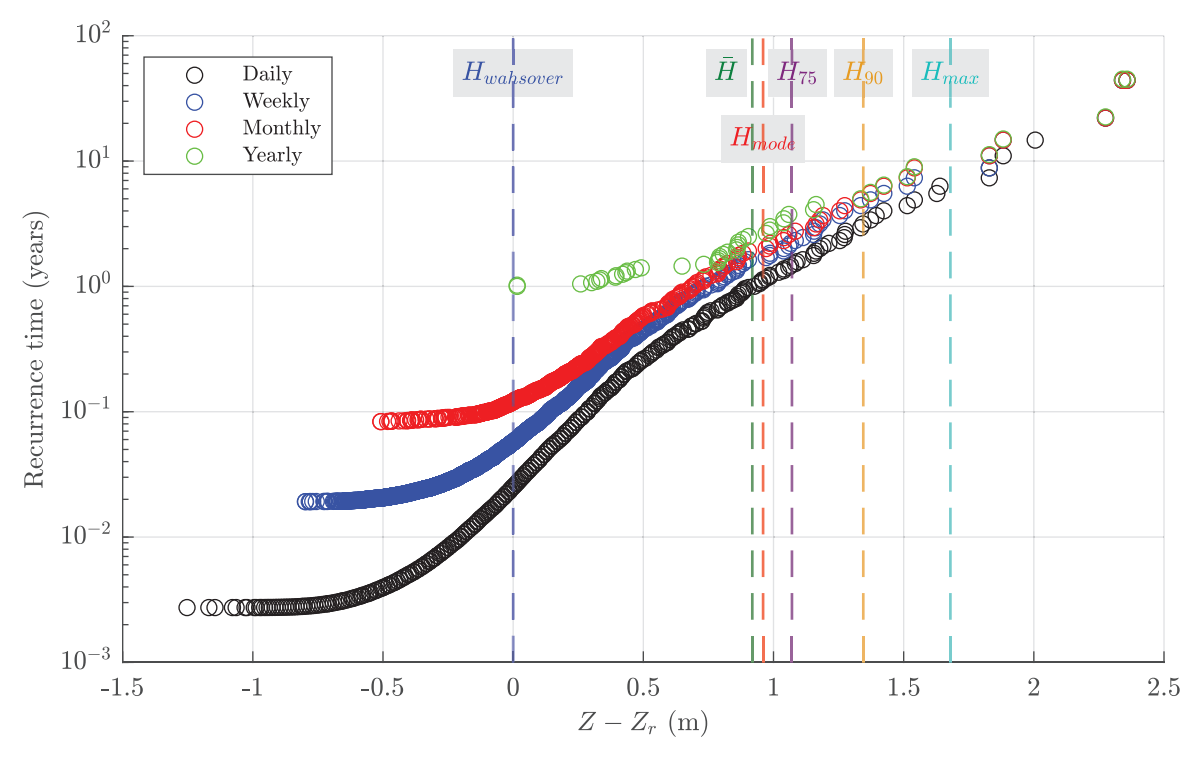


Figure 36: Recurrence time of TWL exceeding given thresholds for different time intervals at Station 42002. The vertical lines indicate key dune metrics: the mode (H_{Mode}), the mean (H_{Mean}), the 90th percentile (H_{90}), the 75th percentile (H_{75}), and the maximum dune height (H_{max}) (see Table 4 and Section 3.1).

Table 8: Relevant elevation levels and their recurrence times for flooding due to HWEs at Station 42002.

Relevant elevation	Height relative to Z_r (m)	Recurrence time of flooding due to HWEs
$H_{ m washover}$	0.0	1 month
$H_{ m Mode}$	0.25	2 months
$H_{ m Mean}$	0.5	4 months
H_{75}	1.0	1 year
H_{90}	1.7	10 years

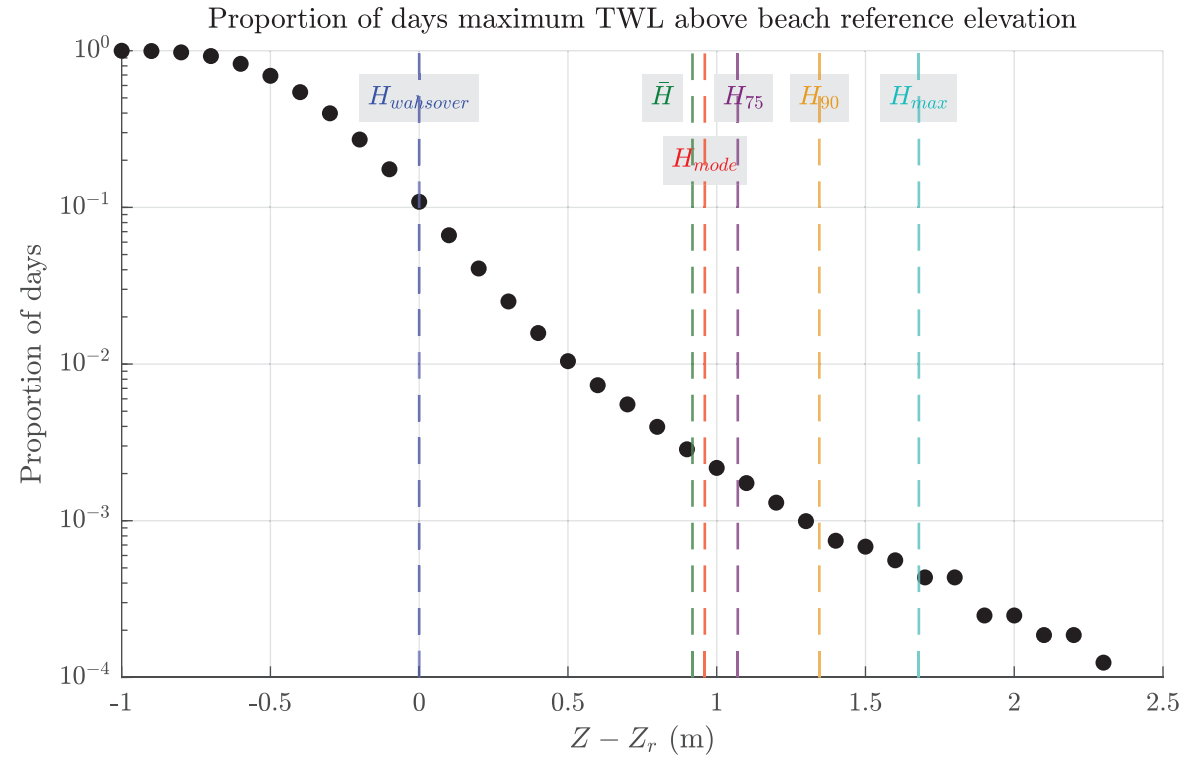


Figure 37: Proportion of days the TWL exceeded given thresholds relative to the reference beach elevation ($Z_r = 1 \text{ m}$, see Section 3.2) at station 42002. The vertical lines indicate key dune metrics: the mode (H_{Mode}), the mean (H_{Mean}), the 90th percentile (H_{90}), the 75th percentile (H_{75}), and the maximum dune height (H_{max}) (see Table 4 and Section 3.1).

5.2 Statistical Properties of HWE

Using the compiled and extended time series of still water levels from Freeport Harbor tidal gauges, along with offshore wave data from multiple buoys (see Section 3.3 and Table 1), we analyzed TWL records with varying levels of data gaps and found that the reference beach elevation (Z_r)—defined as the elevation where high-water events (HWEs) occur approximately 18 times per year ($\lambda_r \approx 18 \,\mathrm{yr}^{-1}$)—is consistently around 1 m (see Figure 38).

The range of mean sizes (\overline{S}) of high-water events exceeding the reference elevation $(Z_r = 1 \text{ m})$, across different wave stations and data gap conditions, was between 0.24 m and 0.31 m. Despite variations in data availability, the \overline{S} values generally remain close to 0.27 m, which was selected as the reference mean size $(\overline{S_r})$ (see Table 9 and Figure 39).

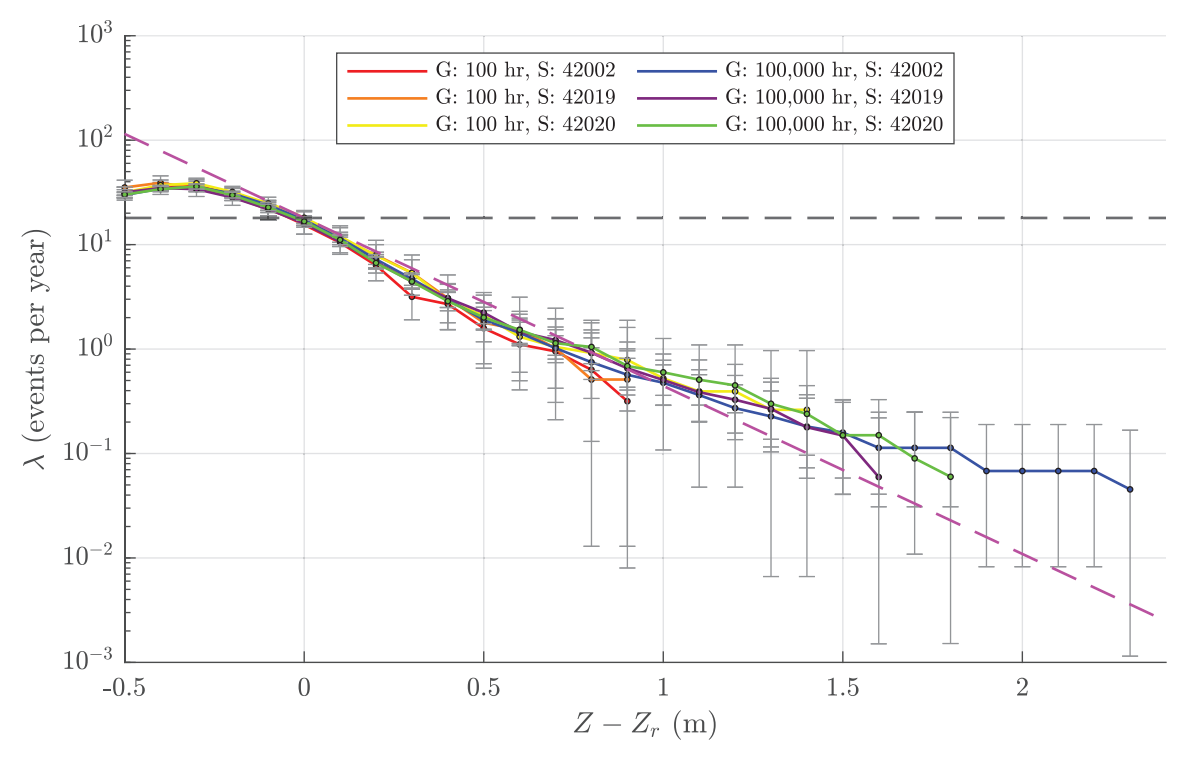


Figure 38: Frequency (λ) of high-water events exceeding elevation Z relative to the reference beach elevation ($Z_r = 1\,\mathrm{m}$; see Section 3.2). The black dashed line shows the prediction from a Poisson process with exponentially distributed sizes, expressed as: $\lambda(Z) = \lambda_r \exp\left(-\frac{Z-Z_r}{S_r}\right)$, where $\lambda_r = 18\,\mathrm{yr}^{-1}$ and $\overline{S_r} = 0.27\,\mathrm{m}$. Different markers represent results from different wave stations (S) and data gap conditions (G) (see Table 1 and Section 3.2).

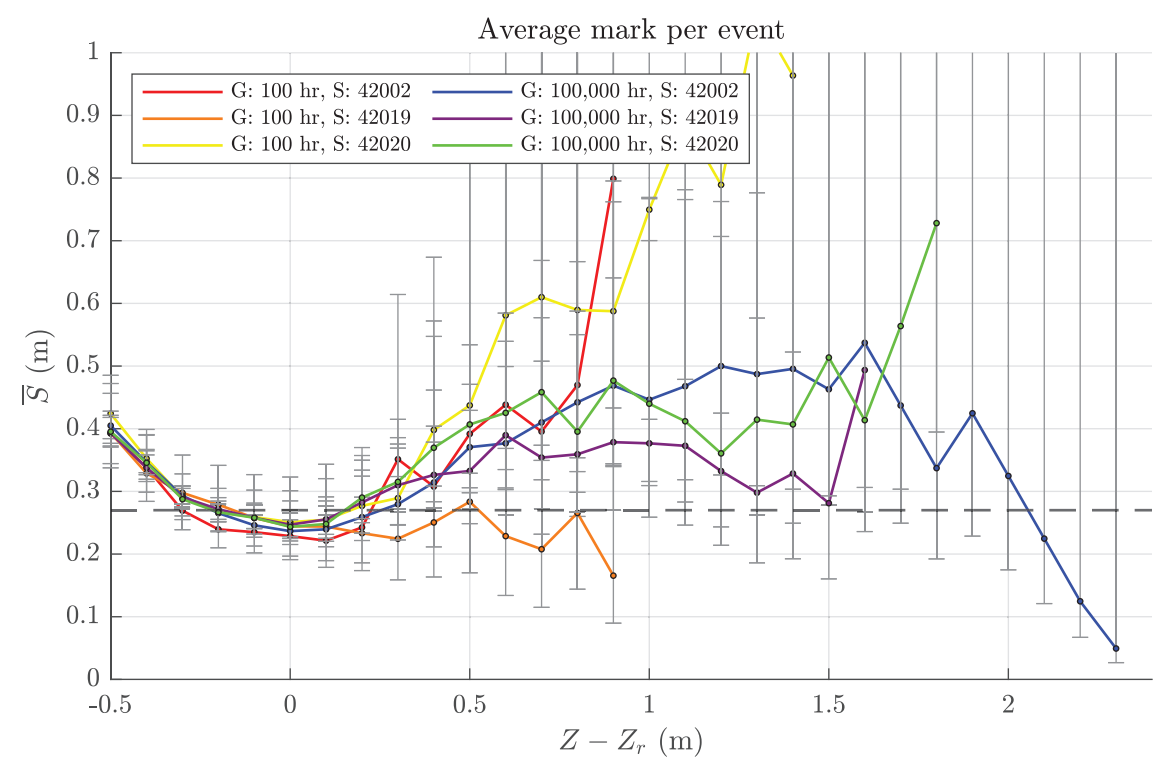


Figure 39: Mean size (\overline{S}) of high-water events exceeding an elevation Z relative to the reference beach elevation $(Z_r = 1 \text{ m}, \text{ see } 3.2))$. The black dashed line represents the corresponding line for $\overline{S_r} = 0.27m$. Different markers represent analyses from different wave stations (S) with varying data gaps (G) (see Table 1 and Section 3.2).

Table 9: Mean size (\overline{S}) of high-water events for different wave stations and data gap conditions.

Wave station	Max gap (hr)	Mean size \overline{S} (m)
42002	100	0.26
42019	100	0.24
42020	100	0.31
42002	100,000	0.28
42019	100,000	0.28
42020	100,000	0.30

5.3 Sediment Transport

We calculated the average total sediment transport rate in all directions and the average onshore-projected component of the transport rate using Equations 13 and 14, respectively. For a wind speed threshold

of 3.5 m/s (see Section 3.4), the average total sediment transport rate in all directions was found to be $15.5 \text{ m}^2/\text{yr}$, and the average onshore-projected component was $12.5 \text{ m}^2/\text{yr}$.

5.4 After-Storm Dune Recovery

As described in Section 3.5, our model predicts that dunes will tend to recover whenever the local elevation capital h_c is above the threshold:

$$h_{cc} = \overline{S} \left(\ln \left(\lambda_r \overline{S} / G_d \right) - 1 \right) \tag{16}$$

where $\lambda_r = 18 \text{yr}^{-1}$, G_d is the maximum (averaged) dune growth rate and \overline{S} is the mean size of HWEs.

In previous sections we estimated the maximum dune growth rate in the range $G_d \approx 0.6 - 0.9$ m/yr (section 4.3.1), and the mean size of HWEs $\overline{S} \approx 0.27$ m (section 5.2). Substituting in the previous equation, the critical elevation capital at this site is in the range 0.2 - 0.3m. Thus, taking the average:

$$h_{cc} \approx 0.25 \text{m} \tag{17}$$

5.4.1 Barrier elevation capital

Elevation capital (h_c) represents the characteristic elevation of the barrier following dune erosion after a major overwash event and serves as a key indicator of its resilience to future disturbances. This elevation is determined by the island's pre-existing morphology, excluding the influence of dune structures.

We define the elevation capital as the lowest elevation of the highest 50 m of the barrier along each cross-shore profile, where the 50 m distance approximately corresponds to the maximum dune width at the site. In our analysis, cross-shore profiles consist of equidistant points spaced 1 m apart; therefore, elevation capital is calculated as the 50th highest elevation within the lateral limits of the barrier for each profile.

Figures 40 and 41, along with Table 10, present the histograms, key metrics, and alongshore profiles of the elevation capital at our site. Figure 41 clearly shows that the elevation capital is lowest in the central washover region.

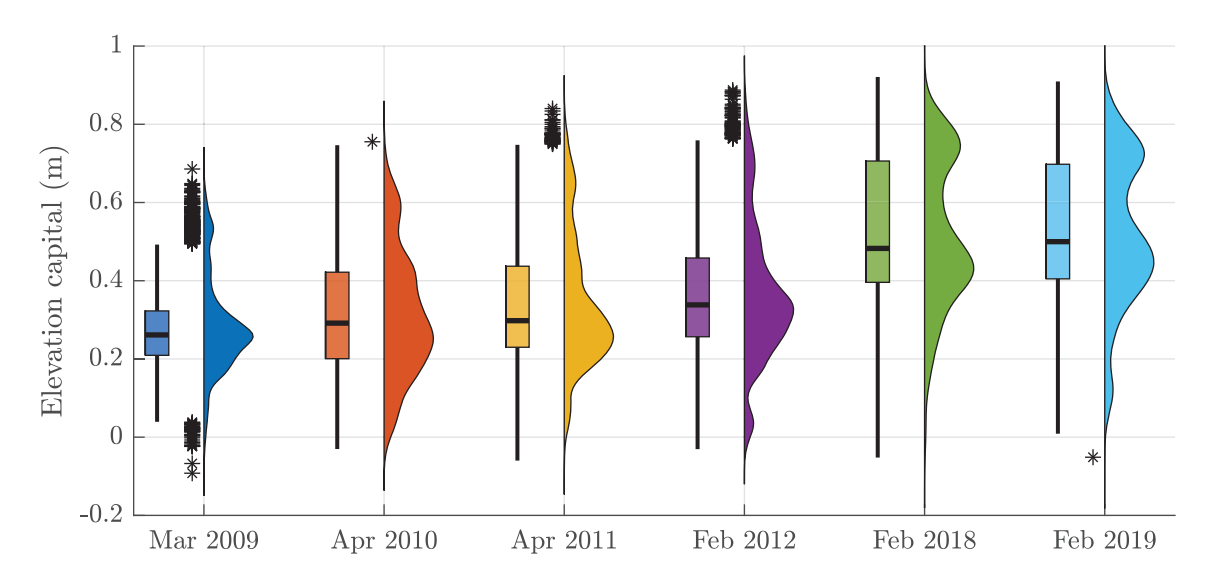


Figure 40: Temporal evolution of elevation capital at the Cedar Lakes site from March 2009 to February 2019. Elevation capital remained relatively stable until 2012, after which it increased due to the increase in barrier width, as expected based on the definition of elevation capital.

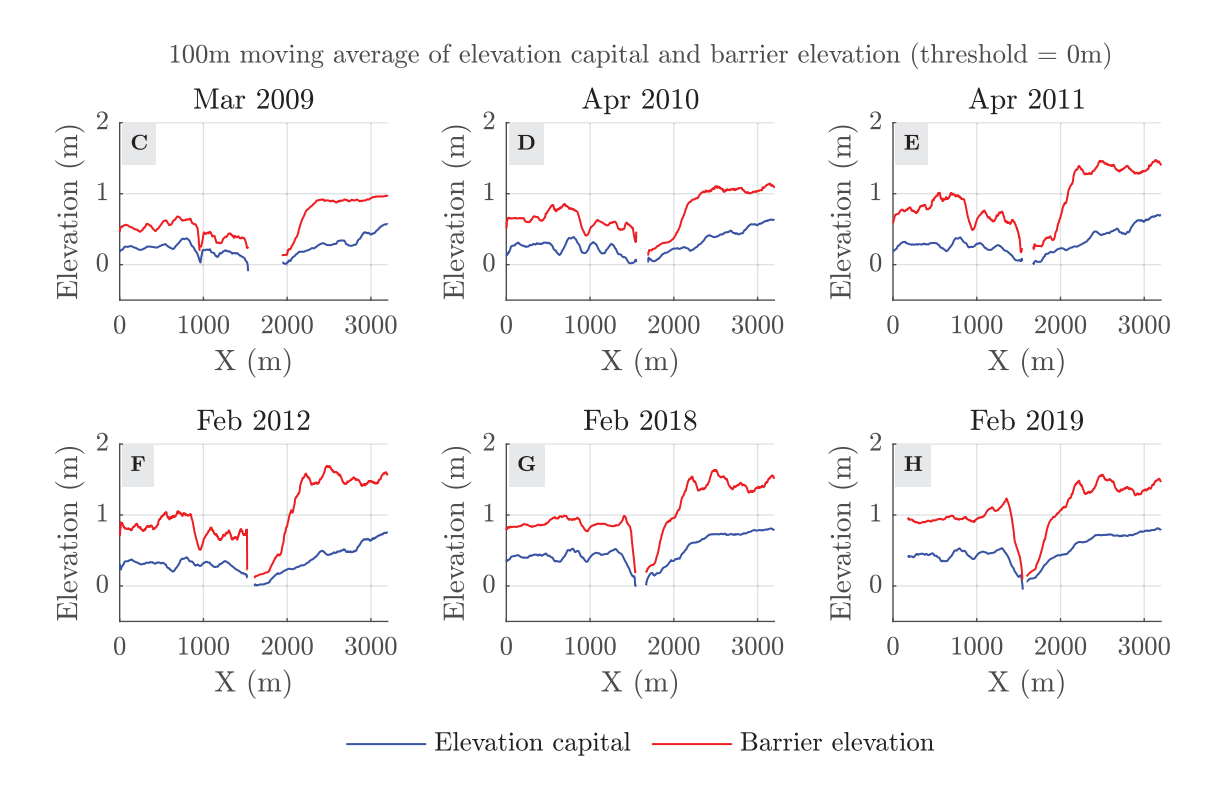


Figure 41: 100m moving average of elevation capital and barrier elevation at the Cedar Lakes site from March 2009 to February 2019. The red line represents barrier elevation, while the blue line represents elevation capital.

Table 10: Summary statistics for the elevation capital (m) distribution: the mode (H_{Mode}) , the mean (H_{Mean}) , the 75th percentile (H_{75}) , the 90th percentile (H_{90}) , and the maximum value (H_{max}) .

Year	$H_{ m Mode}$	$H_{ m Mean}$	H_{75}	H_{90}	$H_{ m max}$
Mar 2009	0.25	0.3	0.3	0.4	0.5
Apr 2010	0.25	0.3	0.4	0.6	0.7
Apr 2011	0.25	0.3	0.4	0.6	0.7
Feb 2012	0.3	0.4	0.4	0.6	0.8
Feb 2018	0.7	0.5	0.7	0.8	0.9
Feb 2019	0.7	0.5	0.7	0.8	0.9

5.4.2 Validation of the Dune Recovery Threshold

Figure 42 shows the relationships between elevation capital and barrier elevation when the data is averaged over 100m alongshore sections. In the figure we set a limit of 0.75m for the local barrier elevation to be considered a mature dune. From the data it is clear that dunes tend to recover whenever the elevation capital is higher than 0.25m, which validates the model prediction.

The model prediction is also confirmed when we analyze the data using 50-meter averaged alongshore sections only in the washover central region and the eastern section of the barrier, and combining all elevations after 2009 (see Figure 43).

In section 5.6, this dune recovery condition ($h_c > 0.25$ m) will be applied to identify alongshore points where dunes cannot recover effectively after storm erosion, and are thus replaced by washovers.

Elevation capital vs barrier elevation (whole region, 100m interval, threshold = 0m)

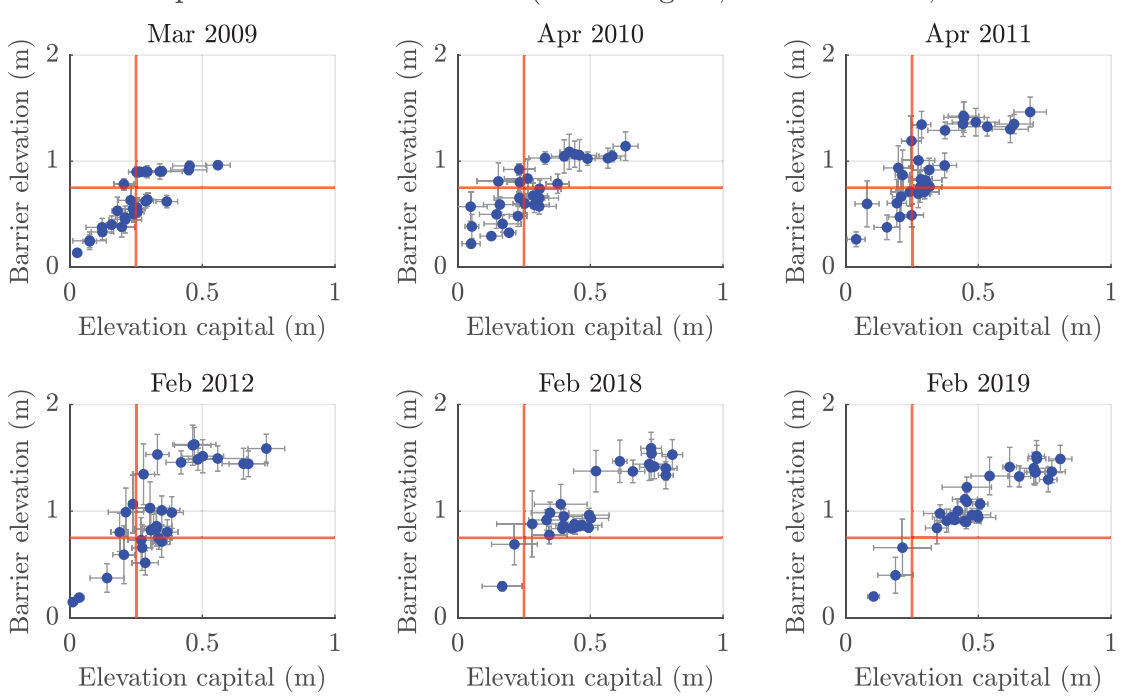


Figure 42: Relationship between elevation capital and barrier elevation, averaged over 100-meter intervals for the entire Cedar Lakes site. Blue markers represent averaged data points, with horizontal and vertical error bars indicating standard deviations of barrier elevation and elevation capital. The red lines denote the reference thresholds: 0.25 m as the critical elevation capital required for dune recovery and 0.75 m as the lower boundary associated with the dune limit. The plot highlights two distinct regions: when elevation capital is below 0.25 m, most points have barrier elevations under 0.75 m, indicating that dunes might not recover and may remain vulnerable to overwash. In contrast, when elevation capital exceeds 0.25 m, most points have elevations above 0.75 m, suggesting that dune recovery and stabilization may be successful.

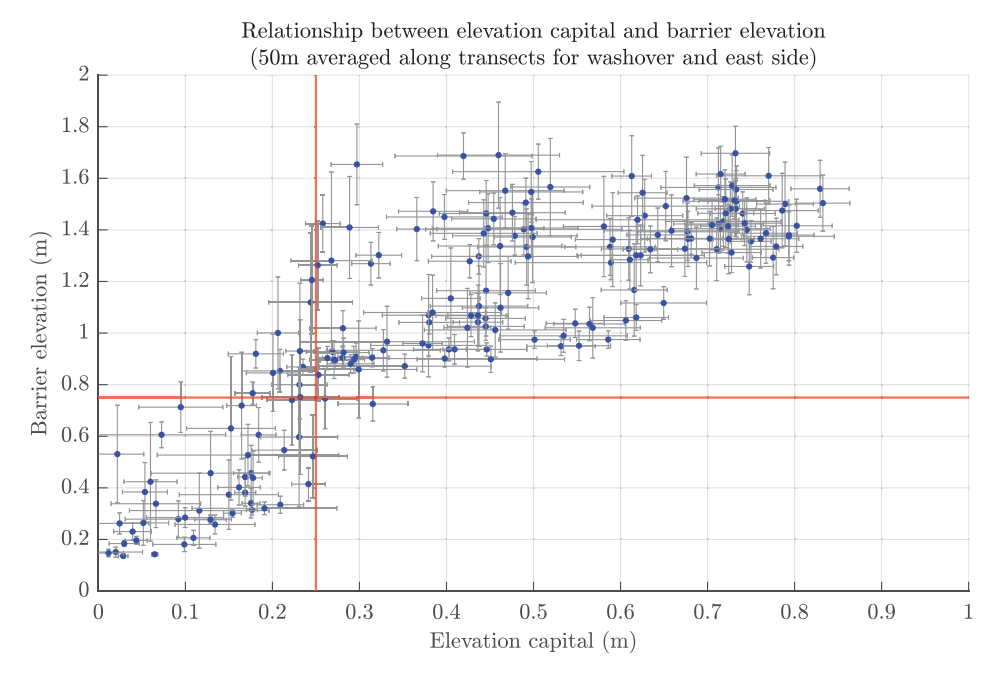


Figure 43: Relationship between elevation capital and barrier elevation, averaged over 50-meter intervals in the washover region and eastern section of the barrier, based on DEMs from post-2009 datasets. Blue markers represent averaged data points, with horizontal and vertical error bars indicating the standard deviations of barrier elevation and elevation capital, respectively. The red lines denote the reference thresholds: 0.25 m as the critical elevation capital required for dune recovery and 0.75 m as the lower boundary associated with the dune limit. The plot highlights two distinct regions: when elevation capital is below 0.25 m, most points have barrier elevations under 0.75 m, indicating that dunes might not recover and may remain vulnerable to overwash. In contrast, when elevation capital exceeds 0.25 m, most points have elevations above 0.75 m, suggesting that dune recovery and stabilization may be successful.

5.5 Barrier Breaching Threshold

We found that the relation between barrier width and elevation capital (averaged over 100m sections, see Fig. 44) can shed light into the conditions for potential barrier breaching during large storms.

Barrier breaching occurs when the total energy associated to the storm surge and run-up overtopping the barrier over the whole duration of the storm exceeds to work required to erode the sand volume of the barrier above the mean water level. It seems plausible that sections with little or no elevation capital $(h_c \lesssim 0, \text{ relative to the beach elevation } Z_r)$ are the most susceptible to breaching. By definition, the condition $h_c \sim 0$ is characterized by a barrier width around 50 m.

Elevation capital vs min barrier width (whole region, 100m interval, threshold = 0m)

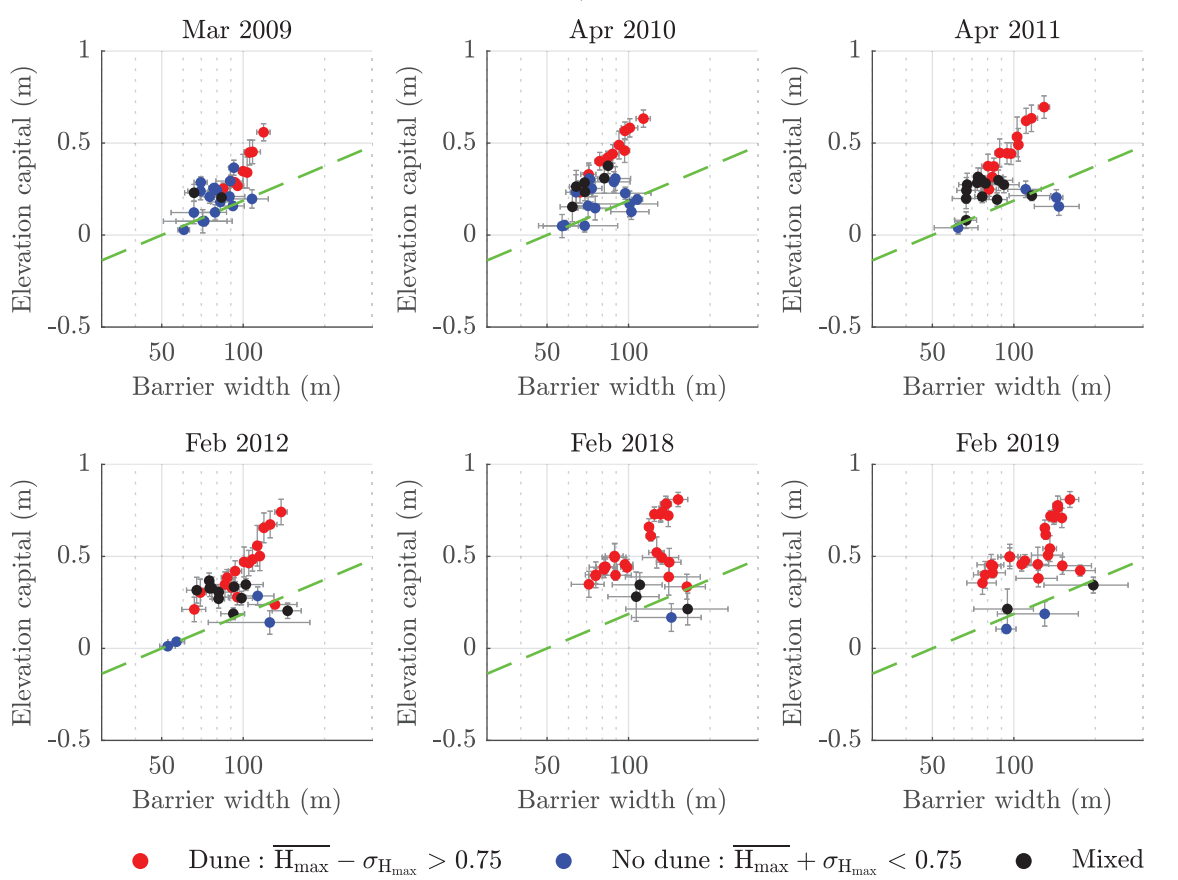


Figure 44: Relationship between elevation capital and barrier width, averaged over 100-meter intervals for the entire Cedar Lakes site. Data points are categorized into three groups: red markers represent dune presence, blue markers indicate no dune formation, and black markers correspond to mixed states. The green dashed line represents the function $y = 0.27 \ln \left(\frac{W}{50} \right)$, where y is the mean elevation capital, and W is the barrier width. The time evolution shows that elevation capital increased over time, leading to the formation of more dunes.

To validate our critical width threshold $W_c \sim 50$ m, we identified alongshore points where the barrier existed in 2012 but was no longer present in 2018, capturing conditions before and after Hurricane Harvey using DEMs. Analyzing these points, we observed a pattern where nearly all points with a barrier width of less than 70 meters in 2012 had disappeared by 2018. Based on this pattern, we established 70 meters as the barrier breaching threshold (Figure 45).

In section 5.6, this threshold is applied to identify alongshore points where the barrier faces increased erosion risk as its width approaches or falls below this limit.

Comparison of barrier elevation and width in the washover region (2012 vs. 2018)

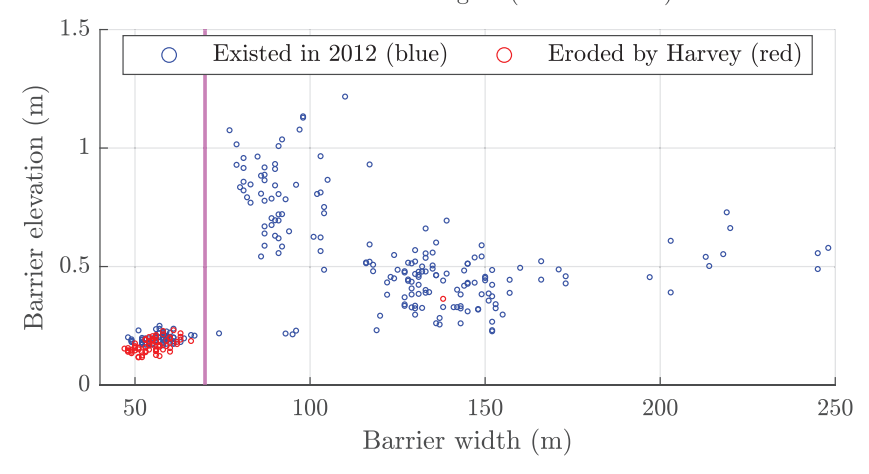


Figure 45: Illustration of breached and unbreached alongshore points in the washover region between 2012 and 2018. Red circles indicate alongshore points where the barrier was breached by Hurricane Harvey and no longer existed in 2018, while blue circles represent alongshore points where the barrier remained intact. Most breached alongshore points, as indicated by the magenta line, had a width of less than 70 meters, distinguishing regions where the barrier failed from those that remained intact. We used 70 meters as the critical barrier breaching threshold.

5.6 Quantification of Dune Recovery and Barrier Breaching for Different Sea Level Rise Scenarios

We quantify dune recovery and barrier breaching using two metrics, the fraction f (Equation 18) of the barrier where dunes can recover, and the fraction f_w (Equation 19) of the barrier susceptible to breaching after an overwash.

The fraction of the barrier where dunes can recover is calculated as

$$f = \frac{N(h_{ci} > h_{cc})}{N_T} \tag{18}$$

where $N(h_{ci} > h_{cc})$ represents the number of alongshore points where the elevation capital exceeds the dune recovery threshold (0.25 m; Section 5.4.2), and N_T is the total number of alongshore points across the barrier island. For example, f = 0.5 means that dunes can recover after a large storm only on half the barrier.

The fraction of the barrier susceptible to breaching is calculated as

$$f_w = \frac{N(W_i < W_c)}{N_T} \tag{19}$$

where $N(W_i < W_c)$ represents the number of alongshore points where the barrier width W_i falls below the critical threshold W_c (70 m; Section 5.5), and N_T is the total number of alongshore points across the barrier

island. For example, $f_w = 0.5$ means that half of the barrier is susceptible to breaching.

We analyzed different SLR scenarios based on projections for 2050, with rates of 1.0 cm/yr, 1.5 cm/yr, and 2.0 cm/yr for moderate, high, and extreme scenarios, respectively, relative to the year 2000, based on NOAA estimates [8] (Table 11). The current local SLR rate for the region is approximately 6.6 mm/yr [4].

OD 11 44	OTD		c	1.00	
Table L	\cdot SLR	rates	tor	different	scenarios.

Scenario	SLR Rate (cm/yr)
Moderate	1.0
Hight	1.5
Extreme	2.0

5.6.1 First Approach

In this approach, we assume that the entire barrier experiences passive inundation while the barrier width remains unchanged. As a result, elevation capital was reduced in response to SLR across different scenarios.

Figure 46 shows the fraction of the barrier length where the dune could recover under different SLR scenarios.

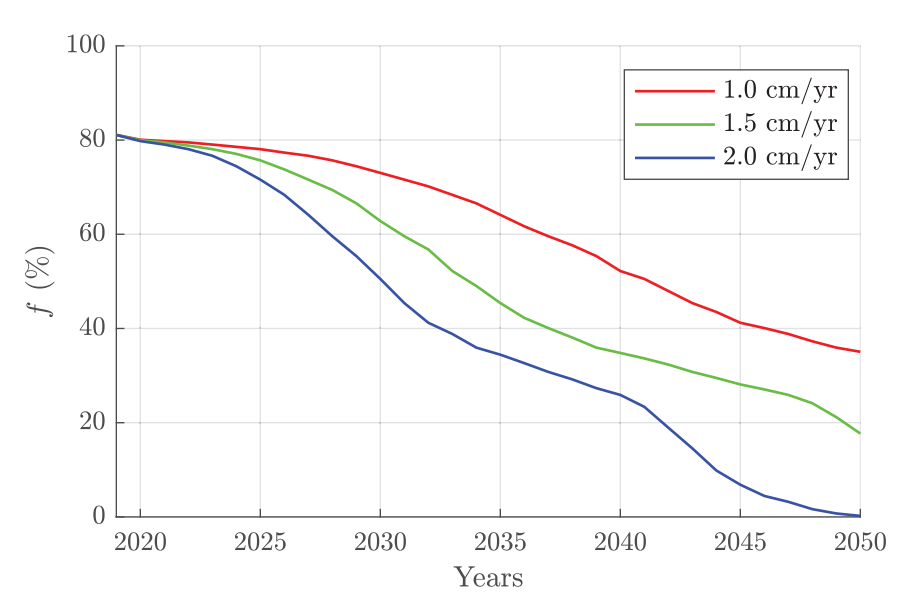


Figure 46: The fraction of the barrier length where the dune could recover, f (Equation 18), based on the first approach, from 2019 to 2050 under three SLR scenarios. These scenarios correspond to rates of 1.0 cm/yr, 1.5 cm/yr, and 2.0 cm/yr, representing moderate, high, and extreme conditions, respectively.

5.6.2 Second Approach

In this approach, we assume that the beach and dune can keep pace with SLR, adapting accordingly, while the back-barrier undergoes passive inundation, which may lead to changes in barrier width.

To ensure a realistic representation of barrier island morphology, we first modified the elevation by implementing a sediment fill condition. Specifically, for each alongshore point, if the horizontal distance between the down-crossing and up-crossing points in the cross-shore profile was less than 5 meters, we assumed that sediment naturally filled this gap, raising the elevation to the beach reference elevation. This process continued iteratively along the cross-shore profile until a stable elevation was identified.

Once the modified elevations were established, we then computed elevation capital and barrier width based on these new conditions and for different SLR scenarios.

Figure 47 illustrates f, the fraction of the barrier length where the dune could recover, while Figure 48 shows f_w , the fraction of the barrier length susceptible to breaching.

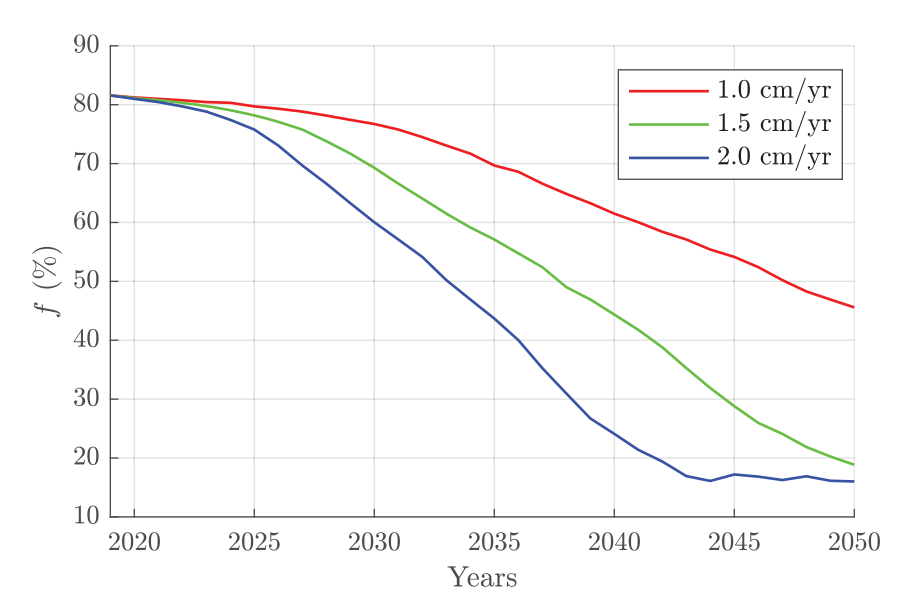


Figure 47: The fraction of the barrier length where the dune could recover, f (Equation 18), based on the second approach, from 2019 to 2050 under three SLR scenarios. These scenarios correspond to rates of 1.0 cm/yr, 1.5 cm/yr, and 2.0 cm/yr, representing moderate, high, and extreme conditions, respectively.

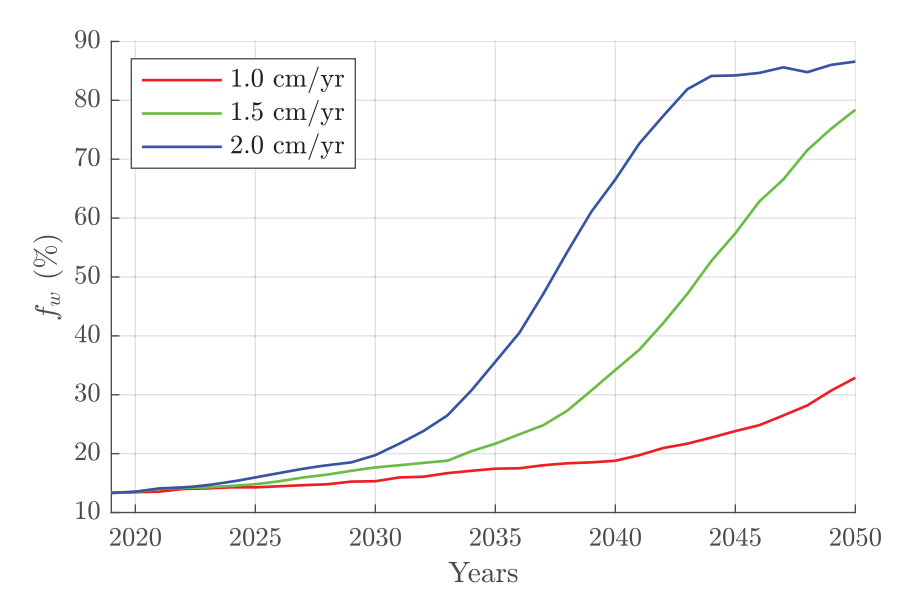


Figure 48: The fraction of the barrier length susceptible to breaching, f_w (Equation 19), based on the second approach, from 2019 to 2050 under three SLR scenarios. These scenarios correspond to rates of 1.0 cm/yr, 1.5 cm/yr, and 2.0 cm/yr, representing moderate, high, and extreme conditions, respectively.

For each alongshore point, we checked two previously defined metrics: the dune recovery threshold (0.25 m; Section 5.4.2), below which the dune may not recover, and the barrier breaching threshold (70 m; Section 5.5), below which the barrier would be susceptible to breaching. If the barrier width was less than the breaching threshold, it was considered vulnerable to breaching under future storm conditions, and points with elevations above zero (relative to Z_r ; Figure 5) were set to zero. Similarly, if the elevation capital was below the dune recovery threshold, dune recovery was assumed to be unlikely, and elevations above 0.75 m (dune limit; Figure 5) were capped at 0.75 m.

We used the 2019 DEM as a starting point and applied the second approach (Section 5.6.2) to project barrier morphology for 2050 under different SLR scenarios. This step generated the initial 2050 DEM, providing a baseline representation of the barrier system's response to SLR before applying threshold-based adjustments. Next, we applied the methodology outlined in the previous paragraph to modify the 2050 DEM, adjusting elevation values where the barrier width or elevation capital fell below critical thresholds. This second modification ensured that the final projected elevation dataset accurately captured the morphological changes driven by future SLR and associated barrier dynamics. The final dataset was then used to generate the projected elevation maps for 2050 under different SLR scenarios.

To provide context, the 2019 baseline map was included for comparison, illustrating the pre-SLR morphology of the study region. The projected maps for 2050 under different SLR conditions are shown in Figures 49, 50, 51, and 52.

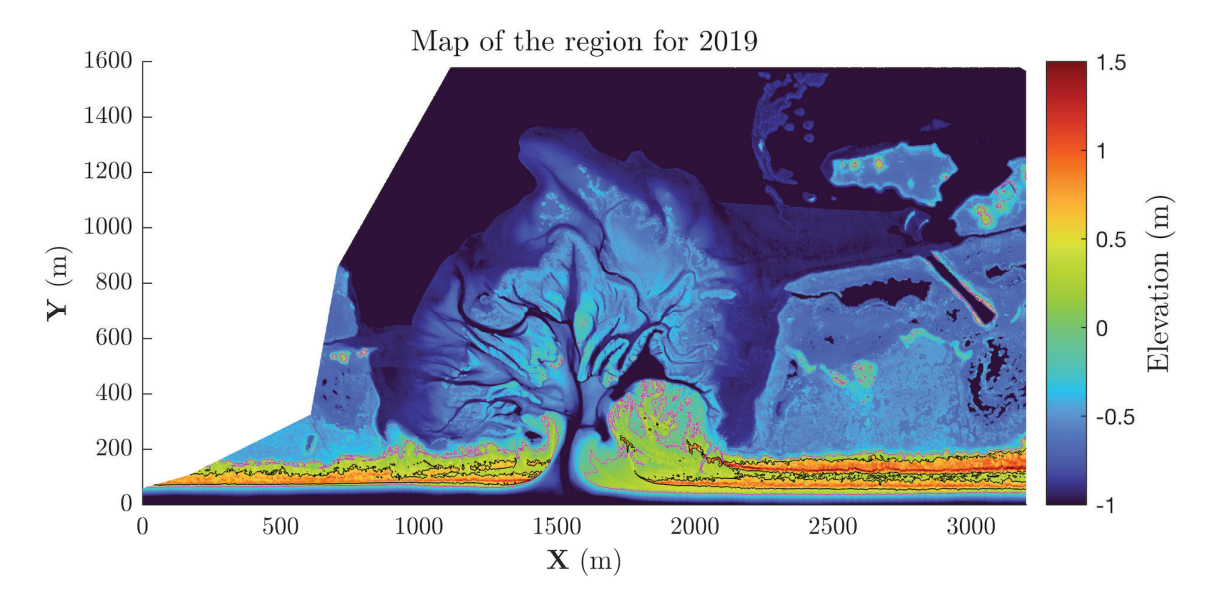


Figure 49: Map of the study region in 2019, showing the initial conditions of the barrier island system before the effects of projected SLR. This serves as a baseline for comparison with future projections under different RSLR scenarios. The magenta line represents the contour line at 0 m (beach), while the black line represents the contour line at 0.5 m (dune region).

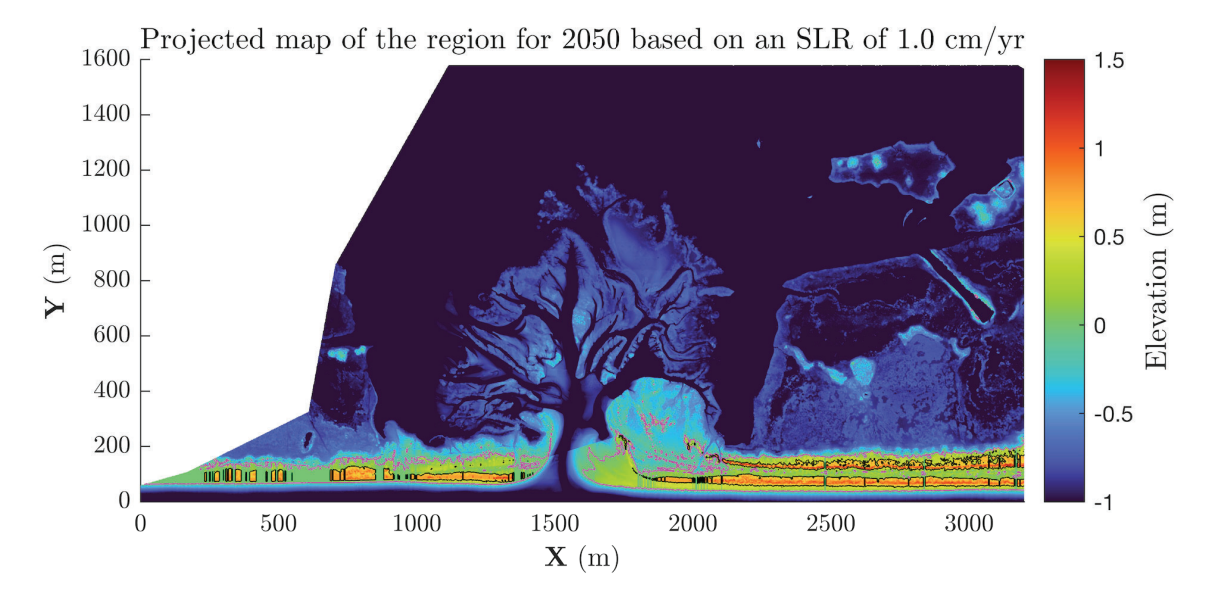


Figure 50: Projected barrier island morphology in 2050 under the intermediate SLR scenario (1.0 cm/yr). The magenta line represents the contour line at 0 m (beach), while the black line represents the contour line at 0.5 m (dune region).

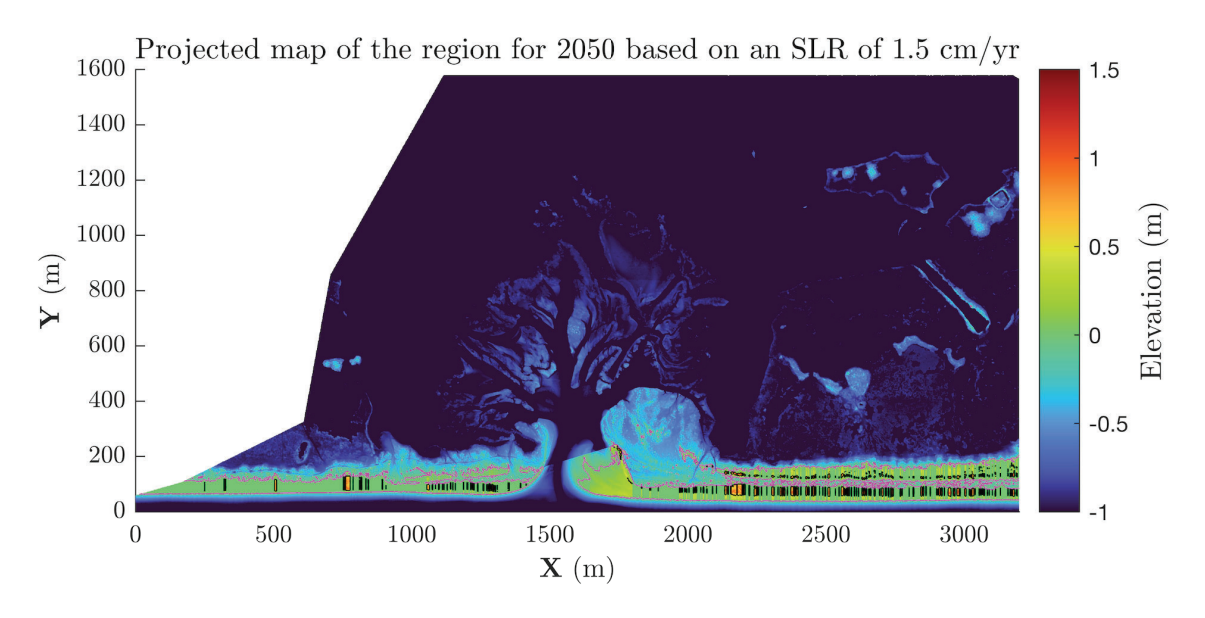


Figure 51: Projected barrier island morphology in 2050 under the high SLR scenario (1.5 cm/yr). The magenta line represents the contour line at 0 m (beach), while the black line represents the contour line at 0.5 m (dune region).

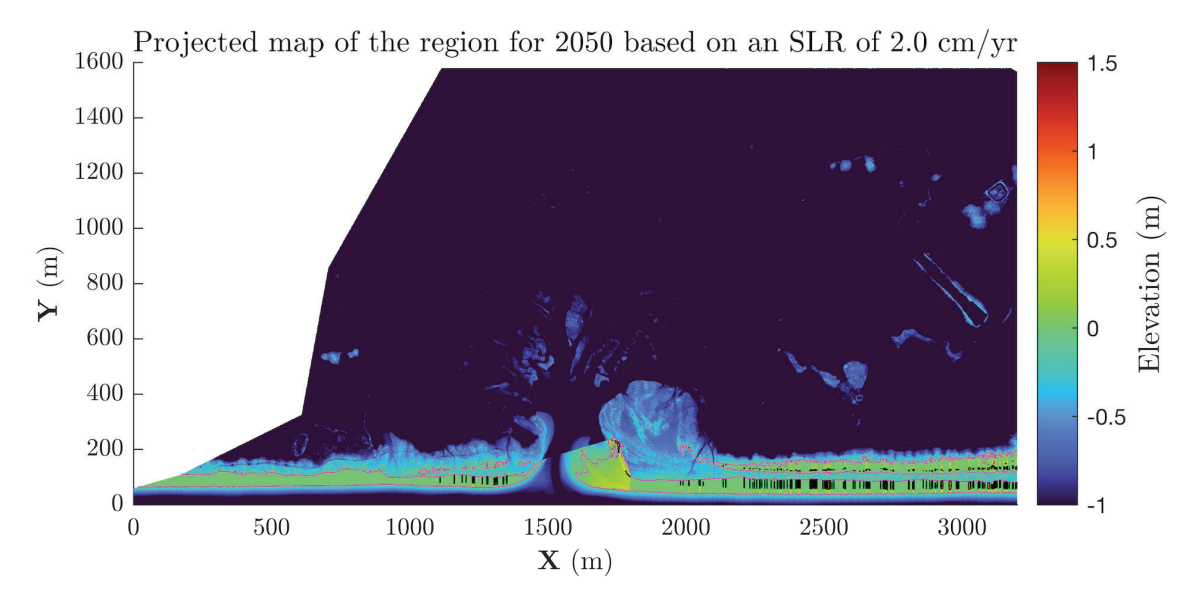


Figure 52: Projected barrier island morphology in 2050 under the extreme SLR scenario (2.0 cm/yr). The magenta line represents the contour line at 0 m (beach), while the black line represents the contour line at 0.5 m (dune region).

References

- [1] O. Durán and L. J. Moore. Vegetation controls on the maximum size of coastal dunes. *Proceedings of the National Academy of Sciences*, 110(43):17217–17222, October 2013.
- [2] Orencio Durán, Philippe Claudin, and Bruno Andreotti. On aeolian transport: Grain-scale interactions, dynamical mechanisms and scaling laws. *Aeolian Research*, 3(3):243–270, 2011.
- [3] Byungho Kang. CNN-Based Imagery Analysis for Monitoring Complex Coastal Processes. Doctoral dissertation, Texas A&M University, 2022.
- [4] NOAA Tides and Currents. Galveston Bay Entrance, North Jetty, TX (Station 8771341), 2025.
- [5] T. Rinaldo, K. A. Ramakrishnan, I. Rodriguez-Iturbe, and O. Durán Vinent. Probabilistic structure of events controlling the after-storm recovery of coastal dunes. *Proceedings of the National Academy of Sciences*, 118(1):e2013254118, 2021.
- [6] H. F. Stockdon, R. A. Holman, P. A. Howd, and A. H. Sallenger Jr. Empirical parameterization of setup, swash, and runup. *Coastal Engineering*, 53(7):573–588, 2006.
- [7] H. F. Stockdon, D. M. Thompson, N. G. Plant, and J. W. Long. Evaluation of wave runup predictions from numerical and parametric models. *Coastal Engineering*, 92:1–11, 2014.
- [8] William V Sweet, Benjamin D Hamlington, Robert E Kopp, Christopher P Weaver, Patrick L Barnard, David Bekaert, William Brooks, Michael Craghan, Gregory Dusek, Thomas Frederikse, et al. Global and regional sea level rise scenarios for the united states: Updated mean projections and extreme weather level probabilities along us coastlines. 2022.
- [9] O. D. Vinent, B. E. Schaffer, and I. Rodriguez-Iturbe. Stochastic dynamics of barrier island elevation. Proceedings of the National Academy of Sciences, 118(1):e2013349118, 2021.

List of Figures

1	Location of the study area (A). Satellite view of the study area (B)	3
2	Time evolution of the Cedar Lakes washover site illustrating dynamic inlet formation and closure over nearly three decades (1995–2023). The sequence of aerial images highlights periods of inlet breaching, sediment deposition, and subsequent natural recovery, emphasizing the transient nature of barrier island morphology. These changes are driven by storm-induced overwash, wave run-up, and sediment transport processes. Understanding these morphological shifts is critical for validating dune recovery models, estimating wave run-up intensity, and assessing coastal resiliency. This site serves as a foundational case study for evaluating the interplay between flooding frequency, after-storm dune recovery, and long-term barrier island stability along the Texas coast	3
3	Timeline of available data from various sources for stations near Cedar Lakes, TX, including satellite imagery, water level records, weather observations, and offshore wave data. Red dashed lines indicate the periods when DEMs and LiDAR data were collected	5
4	Locations of deep-water wave buoys, tidal gauge stations, and weather stations near Cedar Lakes	6
5	Cross-shore profile in Cedar Lakes, Texas, illustrating key coastal morphology metrics. All elevations are referenced to MSL. The barrier width is measured as the distance between the points where the elevation crosses the 1-meter beach reference elevation (Z_r) , while the barrier height corresponds to the maximum elevation within this section, measured relative to Z_r . The pink vertical dotted lines indicate the lateral limits of the barrier. The primary dune is identified as the first crest exceeding the dune base elevation of 0.5 m, closest to the sea. The elevation capital (h_c) represents the island's characteristic elevation following overwash. The solid green horizontal line illustrates the typical overwash length (50 m)	9
6	The plot shows the variation of wind speed (U) over time (t) . The dashed black line represents the transport threshold speed. Points above the threshold $(U > U_t)$, shown in blue, indicate conditions where sediment transport is likely to occur. Points below or at the threshold $(U \le U_t)$, shown in red, indicate conditions where transport does not occur	13
7	Map of the Cedar Lakes site from October 2001, showing key morphological features. The magenta line represents the 0 m contour (beach), while the black line indicates the 0.5 m contour (dune region). These contours provide insight into beach-dune interactions and the potential for overwash and dune recovery.	16

8	Map of the Cedar Lakes site from September 2002, showing key morphological features. The magenta line represents the 0 m contour (beach), while the black line indicates the 0.5 m contour (dune region). These contours provide insight into beach-dune interactions and the potential for overwash and dune recovery	16
9	Map of the Cedar Lakes site from March 2009, showing key morphological features. The magenta line represents the 0 m contour (beach), while the black line indicates the 0.5 m contour (dune region). These contours provide insight into beach-dune interactions and the potential for overwash and dune recovery	16
10	Map of the Cedar Lakes site from April 2010, showing key morphological features. The magenta line represents the 0 m contour (beach), while the black line indicates the 0.5 m contour (dune region). These contours provide insight into beach-dune interactions and the potential for overwash and dune recovery	17
11	Map of the Cedar Lakes site from April 2011, showing key morphological features. The magenta line represents the 0 m contour (beach), while the black line indicates the 0.5 m contour (dune region). These contours provide insight into beach-dune interactions and the potential for overwash and dune recovery	17
12	Map of the Cedar Lakes site from February 2012, showing key morphological features. The magenta line represents the 0 m contour (beach), while the black line indicates the 0.5 m contour (dune region). These contours provide insight into beach-dune interactions and the potential for overwash and dune recovery	17
13	Map of the Cedar Lakes site from February 2018, showing key morphological features. The magenta line represents the 0 m contour (beach), while the black line indicates the 0.5 m contour (dune region). These contours provide insight into beach-dune interactions and the potential for overwash and dune recovery	18
14	Map of the Cedar Lakes site from February 2019, showing key morphological features. The magenta line represents the 0 m contour (beach), while the black line indicates the 0.5 m contour (dune region). These contours provide insight into beach-dune interactions and the potential for overwash and dune recovery	18
15	Growth rate map of the Cedar Lakes site between October 2001 and September 2002. The magenta line represents the 0 m contour (beach), while the black line indicates the 0.5 m contour (dune region). This figure highlights elevation changes and sediment redistribution, providing insights into the short-term morphological evolution of the site	19

Growth rate map of the Cedar Lakes site between April 2010 and April 2011. The magenta line represents the 0 m contour (beach), while the black line indicates the 0.5 m contour (dune region). This figure highlights elevation changes and sediment redistribution, providing insights into the short-term morphological evolution of the site	16	Growth rate map of the Cedar Lakes site between September 2002 and March 2009. The magenta line represents the 0 m contour (beach), while the black line indicates the 0.5 m contour (dune region). This figure highlights elevation changes and sediment redistribution, providing insights into the short-term morphological evolution of the site	19
line represents the 0 m contour (beach), while the black line indicates the 0.5 m contour (dune region). This figure highlights elevation changes and sediment redistribution, providing insights into the short-term morphological evolution of the site	17	line represents the 0 m contour (beach), while the black line indicates the 0.5 m contour (dune region). This figure highlights elevation changes and sediment redistribution, providing	19
line represents the 0 m contour (beach), while the black line indicates the 0.5 m contour (dune region). This figure highlights elevation changes and sediment redistribution, providing insights into the short-term morphological evolution of the site	18	line represents the 0 m contour (beach), while the black line indicates the 0.5 m contour (dune region). This figure highlights elevation changes and sediment redistribution, providing	20
magenta line represents the 0 m contour (beach), while the black line indicates the 0.5 m contour (dune region). This figure highlights elevation changes and sediment redistribution, providing insights into the short-term morphological evolution of the site	19	line represents the 0 m contour (beach), while the black line indicates the 0.5 m contour (dune region). This figure highlights elevation changes and sediment redistribution, providing	20
magenta line represents the 0 m contour (beach), while the black line indicates the 0.5 m contour (dune region). This figure highlights elevation changes and sediment redistribution, providing insights into the short-term morphological evolution of the site	20	magenta line represents the 0 m contour (beach), while the black line indicates the 0.5 m contour (dune region). This figure highlights elevation changes and sediment redistribution,	20
2019, relative to the beach. The barrier height increased from March 2009 to February 2012, followed by a decline in February 2018, likely due to storm-induced erosion. In February 2019, barrier height increased again, suggesting post-storm recovery. The presence of two peaks in some years suggests distinct elevation distributions between the eastern and western sections of the barrier, with the eastern region generally exhibiting higher elevations than the western	21	magenta line represents the 0 m contour (beach), while the black line indicates the 0.5 m contour (dune region). This figure highlights elevation changes and sediment redistribution,	21
	22	2019, relative to the beach. The barrier height increased from March 2009 to February 2012, followed by a decline in February 2018, likely due to storm-induced erosion. In February 2019, barrier height increased again, suggesting post-storm recovery. The presence of two peaks in some years suggests distinct elevation distributions between the eastern and western sections of the barrier, with the eastern region generally exhibiting higher elevations than the western	23
Temporal evolution of barrier width at the Cedar Lakes site from March 2009 to February 2019. During this period, the barrier width increased due to beach accretion	23	·	24

24	Temporal evolution of dune heights relative to the beach at the Cedar Lakes site from March 2009 to February 2019	25
25	Temporal evolution of dune widths at the Cedar Lakes site from March 2009 to February 2019.	26
26	Temporal evolution of dune aspect ratios at the Cedar Lakes site from March 2009 to February 2019. The aspect ratio is defined as the ratio of dune height to width	27
27	Temporal evolution of the alongshore beach-to-dune crest distance at the Cedar Lakes site, computed using a 100-meter moving average.	28
28	Distribution of beach-to-dune crest distances at the Cedar Lakes site	29
29	Relationship between dune height and beach-to-dune crest distance at the Cedar Lakes site. The 2D histogram illustrates a trend where taller dunes are generally associated with greater beach-to-dune crest distances, suggesting a linkage between dune formation processes and sediment transport dynamics. The red line represents the upper bound of dune height predicted by [1]	29
30	Alongshore growth rates averaged over a 100-meter moving window for consecutive intervals. The red line represents the growth rate of maximum elevation, the blue line indicates the growth rate of dune crest elevation, and the green line shows the growth rate of barrier height (see Section 3.1 for definitions of each morphological characteristic). Growth rates range from -0.5 to 0.5 m/yr. Between 2001 and 2002, maximum elevation decreased, followed by a relatively stable period from 2002 to 2009. From 2009 to 2012, maximum elevations increased and washover regions became narrower. During Hurricane Harvey, the washover region widened again, followed by a recovery phase in which it narrowed. From 2018 to 2019, elevations increased on both the western and eastern sides of the barrier	31
31	Relationship between the rate of maximum elevation change (m/yr) and initial elevation at different alongshore locations, relative to the reference beach elevation (see Section 3.2). Individual observations are shown as grey dots, with the average rate for a given initial elevation is shown by the magenta lines. Highlighted points represent the top 10 growth rates observed under two specific conditions: initial elevations above 0 m (beach level; primarily influenced by	
	water-driven processes, red squares) and initial elevations above 0.5 m (dune base; primarily influenced by wind-driven processes, blue plus signs)	32

32	Comparison of sediment volume change rates across consecutive time intervals. Rates were calculated for each cross-shore profile from the shoreline to the center of the barrier. The red horizontal line represents the average onshore-projected sediment transport rate of 12.5 m ² /yr, calculated using Equation 14 for a wind speed threshold of 3.5 m/s (see Section 5.3). Following Hurricane Harvey, the beach recovered at a rate consistent with the transport rate estimated for the same period	34
33	Temporal distribution of sediment volume change rates at the Cedar Lakes site from March 2009 to February 2019	35
34	Distribution of TWL at the station 42002 for different time intervals	37
35	Recurrence time of TWL exceeding given thresholds for different time intervals. The vertical lines indicate key dune metrics: the mode (H_{Mode}) , the mean (H_{Mean}) , the 90th percentile (H_{90}) , the 75th percentile (H_{75}) , and the maximum dune height (H_{max}) (see Table 4 and Section 3.1). Different markers represent analyses from different wave stations (S) with varying data gaps (G) (see Table 1 and Section 3.2)	38
36	Recurrence time of TWL exceeding given thresholds for different time intervals at Station 42002. The vertical lines indicate key dune metrics: the mode (H_{Mode}) , the mean (H_{Mean}) , the 90th percentile (H_{90}) , the 75th percentile (H_{75}) , and the maximum dune height (H_{max}) (see Table 4 and Section 3.1)	39
37	Proportion of days the TWL exceeded given thresholds relative to the reference beach elevation $(Z_r = 1 \text{ m}, \text{ see Section 3.2})$ at station 42002. The vertical lines indicate key dune metrics: the mode (H_{Mode}) , the mean (H_{Mean}) , the 90th percentile (H_{90}) , the 75th percentile (H_{75}) , and the maximum dune height (H_{max}) (see Table 4 and Section 3.1)	40
38	Frequency (λ) of high-water events exceeding elevation Z relative to the reference beach elevation $(Z_r = 1 \mathrm{m}; \mathrm{see} \mathrm{Section} 3.2)$. The black dashed line shows the prediction from a Poisson process with exponentially distributed sizes, expressed as: $\lambda(Z) = \lambda_r \exp\left(-\frac{Z-Z_r}{\overline{S_r}}\right)$, where $\lambda_r = 18 \mathrm{yr}^{-1}$ and $\overline{S_r} = 0.27 \mathrm{m}$. Different markers represent results from different wave stations (S) and data gap conditions (G) (see Table 1 and Section 3.2)	41
39	Mean size (\overline{S}) of high-water events exceeding an elevation Z relative to the reference beach elevation $(Z_r = 1 \text{ m}, \text{ see } 3.2))$. The black dashed line represents the corresponding line for $\overline{S_r} = 0.27m$. Different markers represent analyses from different wave stations (S) with varying data gaps (G) (see Table 1 and Section 3.2)	42
40	Temporal evolution of elevation capital at the Cedar Lakes site from March 2009 to February 2019. Elevation capital remained relatively stable until 2012, after which it increased due to the increase in barrier width, as expected based on the definition of elevation capital	44

41	100m moving average of elevation capital and barrier elevation at the Cedar Lakes site from March 2009 to February 2019. The red line represents barrier elevation, while the blue line represents elevation capital	44
42	Relationship between elevation capital and barrier elevation, averaged over 100-meter intervals for the entire Cedar Lakes site. Blue markers represent averaged data points, with horizontal and vertical error bars indicating standard deviations of barrier elevation and elevation capital. The red lines denote the reference thresholds: 0.25 m as the critical elevation capital required for dune recovery and 0.75 m as the lower boundary associated with the dune limit. The plot highlights two distinct regions: when elevation capital is below 0.25 m, most points have barrier elevations under 0.75 m, indicating that dunes might not recover and may remain vulnerable to overwash. In contrast, when elevation capital exceeds 0.25 m, most points have elevations above 0.75 m, suggesting that dune recovery and stabilization may be successful.	46
43	Relationship between elevation capital and barrier elevation, averaged over 50-meter intervals in the washover region and eastern section of the barrier, based on DEMs from post-2009 datasets. Blue markers represent averaged data points, with horizontal and vertical error bars indicating the standard deviations of barrier elevation and elevation capital, respectively. The red lines denote the reference thresholds: 0.25 m as the critical elevation capital required for dune recovery and 0.75 m as the lower boundary associated with the dune limit. The plot highlights two distinct regions: when elevation capital is below 0.25 m, most points have barrier elevations under 0.75 m, indicating that dunes might not recover and may remain vulnerable to overwash. In contrast, when elevation capital exceeds 0.25 m, most points have elevations above 0.75 m, suggesting that dune recovery and stabilization may be successful.	47
44	Relationship between elevation capital and barrier width, averaged over 100-meter intervals for the entire Cedar Lakes site. Data points are categorized into three groups: red markers represent dune presence, blue markers indicate no dune formation, and black markers correspond to mixed states. The green dashed line represents the function $y = 0.27 \ln \left(\frac{W}{50} \right)$, where y is the mean elevation capital, and W is the barrier width. The time evolution shows that elevation capital increased over time, leading to the formation of more dunes	48
45	Illustration of breached and unbreached alongshore points in the washover region between 2012 and 2018. Red circles indicate alongshore points where the barrier was breached by Hurricane Harvey and no longer existed in 2018, while blue circles represent alongshore points where the barrier remained intact. Most breached alongshore points, as indicated by the magenta line, had a width of less than 70 meters, distinguishing regions where the barrier failed from those that remained intact. We used 70 meters as the critical barrier breaching threshold	49

46	The fraction of the barrier length where the dune could recover, f (Equation 18), based on the first approach, from 2019 to 2050 under three SLR scenarios. These scenarios correspond to rates of 1.0 cm/yr, 1.5 cm/yr, and 2.0 cm/yr, representing moderate, high, and extreme conditions, respectively	50
47	The fraction of the barrier length where the dune could recover, f (Equation 18), based on the second approach, from 2019 to 2050 under three SLR scenarios. These scenarios correspond to rates of 1.0 cm/yr, 1.5 cm/yr, and 2.0 cm/yr, representing moderate, high, and extreme conditions, respectively	51
48	The fraction of the barrier length susceptible to breaching, f_w (Equation 19), based on the second approach, from 2019 to 2050 under three SLR scenarios. These scenarios correspond to rates of 1.0 cm/yr, 1.5 cm/yr, and 2.0 cm/yr, representing moderate, high, and extreme conditions, respectively	52
49	Map of the study region in 2019, showing the initial conditions of the barrier island system before the effects of projected SLR. This serves as a baseline for comparison with future projections under different RSLR scenarios. The magenta line represents the contour line at 0 m (beach), while the black line represents the contour line at 0.5 m (dune region)	53
50	Projected barrier island morphology in 2050 under the intermediate SLR scenario (1.0 cm/yr). The magenta line represents the contour line at 0 m (beach), while the black line represents the contour line at 0.5 m (dune region)	53
51	Projected barrier island morphology in 2050 under the high SLR scenario (1.5 cm/yr). The magenta line represents the contour line at 0 m (beach), while the black line represents the contour line at 0.5 m (dune region)	54
52	Projected barrier island morphology in 2050 under the extreme SLR scenario (2.0 cm/yr). The magenta line represents the contour line at 0 m (beach), while the black line represents the contour line at 0.5 m (dune region).	54

List of Tables

1	$List\ of\ station\ IDs,\ names,\ and\ characteristics\ for\ wave\ buoys,\ tidal\ gauges,\ and\ weather\ stations.$	6
2	Summary statistics for the barrier height (m) distribution relative to the beach: the mode (H_{Mode}) , the mean (H_{Mean}) , the 75th percentile (H_{75}) , the 90th percentile (H_{90}) , and the maximum value (H_{max})	23
3	Summary statistics for the barrier width (m) distribution: the mode (W_{Mode}) , the mean (W_{Mean}) , the 75th percentile (W_{75}) , the 90th percentile (W_{90}) , and the maximum value (W_{max}) .	24
4	Summary statistics for the dune height (m) distribution relative to the beach: the mode (H_{Mode}) , the mean (H_{Mean}) , the 75th percentile (H_{75}) , the 90th percentile (H_{90}) , and the maximum value (H_{max})	25
5	Summary statistics for the dune width (m) distribution: the mode (W_{Mode}) , the mean (W_{Mean}) , the 75th percentile (W_{75}) , the 90th percentile (W_{90}) , and the maximum value (W_{max})	26
6	Summary statistics for the dune aspect ratio distribution: the mode (A_{Mode}) , the mean (A_{Mean}) , the 75th percentile (A_{75}) , the 90th percentile (A_{90}) , and the maximum value (A_{max}) .	27
7	Average and top 10 average growth rates of maximum elevation change (m/yr), based on the highlighted points in Figure 31. The first column shows the average growth rate for locations where the initial elevation ranged between 0.5 and 1 m above the reference beach elevation (see Section 3.2). The second column presents the top 10 average growth rates for locations with initial elevations greater than 0 m (beach level; primarily influenced by water-driven processes). The third column shows the top 10 average growth rates for locations with initial elevations exceeding 0.5 m (dune base; primarily influenced by wind-driven processes	33
8	Relevant elevation levels and their recurrence times for flooding due to HWEs at Station 42002.	39
9	Mean size (\overline{S}) of high-water events for different wave stations and data gap conditions	42
10	Summary statistics for the elevation capital (m) distribution: the mode (H_{Mode}) , the mean (H_{Mean}) , the 75th percentile (H_{75}) , the 90th percentile (H_{90}) , and the maximum value (H_{max}) .	45
11	SLR rates for different scenarios	50